AIMS Materials Science, 12(6): 1176–1214.
DOI: 10.3934/matersci.2025055
Received: 03 September 2025
Revised: 16 November 2025
Accepted: 26 November 2025
Published: 04 December 2025

https://www.aimspress.com/journal/Materials

Review

Preparation and application of lightweight and high-strength ceramsite derived from solid waste in lightweight concrete: A review

Haipeng Liu[1], Nanyan Hu[1,2,*], Qigao Li[3], Shengwen Yang[3], Yicheng Ye[1,2], Jie Wang[4] and Hongping Wang[3]

[1] School of Resources and Environmental Engineering, Wuhan University of Science and Technology, Wuhan, Hubei Province, 430081, China
[2] Hubei Key Laboratory for Efficient Utilization and Agglomeration of Metallurgic Mineral Resources, Wuhan University of Science and Technology, Wuhan, 430081, China
[3] China First Metallurgical Group Co., LTD, Wuhan, 430081, China
[4] Anhui Wanbao Mining Co., LTD, Chizhou, 247100, Anhui Province, China

* **Correspondence:** Email: hunanyan@wust.edu.cn; Tel.: +86-134-2982-8413.

Abstract: As a green lightweight aggregate, solid waste-based ceramsite was significant for decarbonizing building materials. This review systematically summarized its preparation processes, centered on sintered and non-sintered technologies, performance regulation mechanisms, and applications in lightweight concrete. Existing research indicated that raw material formulation, additive type, and curing process collectively governed macroscopic properties such as apparent density, strength, and water absorption by controlling the phase composition and microstructure of ceramsite. In terms of environmental benefits, solid waste-based ceramsite exhibited notable heavy metal immobilization capacity and reduced energy consumption and carbon footprint by utilizing inherent energy from solid waste and optimizing sintering processes. Currently, sintered ceramsite demonstrated superior strength and durability, while non-sintered ceramsite offered advantages of low energy consumption and simple processing, though its strength and functionality required further enhancement. Future research was suggested to focus on multi-property synergy mechanisms, long-term durability assessment, and low-temperature efficient activation technologies to promote the large-scale application of solid waste-based ceramsite in construction materials.

Keywords: solid waste-based ceramsite; preparation processes; factors influencing performance; heavy metal solidification; lightweight concrete

1. Introduction

Lightweight high-strength concrete (LWHSC) was prepared using lightweight aggregates and had a 28-day compressive strength greater than 40 MPa with an oven-dry density less than 1950 kg/m^3 [1]. It possesses low dead load, exceptional strength, reduced thermal conductivity, and excellent heat resistance [2–4]. These attributes render it exceptionally well-suited for fulfilling the performance criteria of tall buildings and structures with extensive spans [5]. Moreover, LWHSC also contributes to the seismic damping of buildings [6], thus offering extensive prospects for engineering applications [7,8].

Ceramsite is a common lightweight aggregate for high-strength lightweight concrete, whose strength and apparent density directly determine the macroscopic properties of concrete, with the former governing compressive strength and the latter restricting dry density [9–11]. Furthermore, multiple studies expanded the application scenarios of concrete by designing the functionality of ceramsite: Bekkeri et al. found that the density of concrete decreased with the increase in artificial aggregate replacement level, and the prepared ceramsite concrete achieved a 90-day compressive strength of over 43.56 MPa, making it suitable for structural applications [12]. Zhou et al. discovered that incorporating 1.5% of 9 mm fibers into spherical aggregates resulted in a cylinder compressive strength of 65.09 MPa. Using these as aggregates to produce concrete not only enhanced its flexural strength but also improved its compressive plastic deformation capacity, enabling it to meet the dual requirements of strength and deformation performance for backfill materials in goaf areas [13]. Jiang et al. found that carbonated recycled coarse aggregates had a lower density, and the concrete prepared with them exhibited significantly improved resistance to chloride penetration and service life, making it suitable for the construction and maintenance of marine infrastructure [14]. Ying et al. developed multi-stage phase-change concrete using coated phase-change ceramsite. They observed that the compressive strength of the concrete decreased as the content of phase-change aggregate increased; however, the concrete demonstrated effective thermal regulation at multiple temperature points between 5 and 15 °C, indicating significant application potential for mitigating frost heave in subgrades in cold regions [15]. In summary, concrete prepared with ceramsite as a lightweight aggregate exhibited excellent performance in strength, durability, and functionality, and has been widely used in fields such as building construction, roadway support, marine engineering, and road construction.

The development of ceramsite underwent a fundamental shift from reliance on natural raw materials to the predominant use of solid waste. In recent years, to promote the resource utilization of solid waste and in response to environmental policies such as the clay prohibition, the use of solid wastes like fly ash, sludge, and tailings with similar compositions became the mainstream direction for ceramsite production [16–18]. Bibliometric data strongly corroborated this trend: over the past decade, research on solid waste-based ceramsite showed explosive growth, with publication growth rates of 667.14% in Web of Science (WOS) and 3066.67% in China National Knowledge Infrastructure (CNKI), which highlighted the increasing research attention and importance of this field. Using modern techniques such as pelletization and high-temperature sintering (or non-sintered curing processes) [19,20], these solid wastes were processed into lightweight, high-strength

aggregates characterized by a hard shell and porous interior. Consequently, these ceramsites exhibited excellent properties like low density, high strength, and corrosion resistance, leading to broad application prospects [21–23]. The focus of future research will be on expanding their applications to achieve higher value-added utilization.

This review systematically elucidates the preparation principles, performance regulation, application prospects, and environmental safety analysis of solid waste-based ceramsite, centered on sintering and non-sintering technologies. It first analyzes how key factors such as raw material formulation and additives govern ceramsite properties by modulating phase composition and microstructure, and further reveals the distinct mechanisms involved, including high-temperature phase evolution and structural formation in sintered ceramsite, and chemical bonding along with hydration product formation in non-sintered ceramsite. The review then demonstrates the excellent performance and engineering advantages of the resulting lightweight high-strength ceramsite in concrete applications across various fields such as building construction, mine support, marine engineering, and road infrastructure. In terms of environmental benefits, quantitative analyses of energy consumption and carbon footprint validate the clean production potential of solid waste-based ceramsite; combined with heavy metal immobilization mechanisms and pollutant control strategies, its environmental safety is confirmed from a life cycle perspective. Finally, the review summarizes future development pathways for solid waste-based ceramsite and offers a forward-looking perspective, aiming to provide a theoretical basis and practical guidance for the development and application of green low-carbon building materials.

2. Preparation and environmental benefit analysis of solid waste-based ceramsite

2.1. Production of ceramsite using solid waste materials

2.1.1. Raw materials for preparation

The utilization of solid waste for ceramsite production represented a crucial approach to addressing environmental requirements and promoting sustainable development. Specifically, bulk solid wastes suitable for manufacturing lightweight high-strength ceramsite included mining tailings, industrial slag, engineering muck, and silt/sludge [24–27]. The primary chemical components of these solid wastes consisted of oxides such as SiO_2, Al_2O_3, Fe_2O_3, CaO, MgO, K_2O, and Na_2O, which provided a compositional basis for their resource utilization. Since the composition of a single solid waste often proved insufficient, two or more types were typically blended and formulated to optimize the overall chemical composition. The produced ceramsites exhibited excellent key properties including density, strength, and water absorption, meeting the Chinese national standards for use as lightweight aggregates [28]. Zhang et al. successfully sintered lightweight ceramsite using molybdenum tailings, iron tailings, and waste glass powder, which achieved a bulk density of 427.2 kg/m^3 and a compressive strength of 5.03 MPa [29]. Zeng et al. produced Grade 600 ceramsite from stone coal leaching residue, bauxite residue, and feldspar, which exhibited a bulk density of 594.3 kg/m^3, a compressive strength of 7.33 MPa, and a 1-hour water absorption of 4.96%, thus meeting the relevant Chinese standard [30]. Kang et al. prepared lightweight high-strength sintered ceramsite from engineering muck, fly ash, and stone powder, which exhibited a water absorption rate not exceeding 12.6%, a density grade of 700, and a cylinder compressive strength of

not less than 5.5 MPa [31]. Fei et al. produced high-strength ceramsite from oily sludge and cuttings cake. The resulting ceramsite achieved a bulk density of 718 kg/m^3, a cylinder compressive strength of 10.94 MPa, and a water absorption of 7.30%, meeting the Grade 800 requirements of the Chinese national standard [32].

The production of lightweight high-strength ceramsite imposed specific chemical requirements on the solid wastes used. According to the Riley phase diagram (Figure 1), the suitable chemical composition ranges for producing expanded ceramsite were: 53%–79% SiO_2, 10%–25% Al_2O_3, and 13%–26% fluxing oxides [33]. In studies on the preparation of lightweight high-strength ceramsite, the raw material components of solid wastes were classified into three categories according to their functions: ceramic-forming components, fluxing components, and gas-generating components [34]. The ceramic-forming components, SiO_2 and Al_2O_3, collectively formed a stable aluminosilicate network, serving as the skeletal framework and strength-regulating constituent, respectively. Amorphous SiO_2 was the primary component of the ceramsite skeletal structure and facilitated the formation of a liquid phase during the sintering process [35]. When the Al_2O_3 content exceeded the threshold of 18 wt%, it promoted the formation of mullite ($3Al_2O_3 \cdot 2SiO_2$), whose interlocked needle-like microstructure significantly enhanced mechanical robustness [36]. Furthermore, an appropriate SiO_2/Al_2O_3 ratio contributed to optimized high-temperature liquid phase behavior, thereby enabling effective expansion of the ceramsite during sintering. Liu et al. conducted a study using low-silica red mud and supplementary sintering materials. Their results indicated that ceramsite prepared with a Si/Al ratio of 1.376 exhibited a uniform porous structure and demonstrated excellent environmental compatibility [37]. Flux components (CaO, MgO, K_2O, Na_2O, Fe_2O_3) regulated melting behavior, promoted liquid phase formation, and thereby achieved structural densification during ceramsite sintering. Studies revealed distinct mechanisms for different oxides: Xiao et al. found that MgO reacted with SiO_2 to form magnesium silicate, which enhanced the expansion capacity of ceramsite. In contrast, Na_2O promoted quartz melting and albite formation, consequently reducing compressive strength [38]. Qin et al. reported that CaO addition significantly decreased endothermic effects during heating, effectively lowered the sintering temperature, and facilitated the formation of new phases [39]. Sun et al. further demonstrated that increasing Fe_2O_3 content gradually reduced liquid phase content and viscosity, while broadening the melting temperature range [40]. Yang et al. also confirmed that higher K_2O content contributed to an expanded sintering temperature range [41]. Gas-generating components (such as organic carbon, calcite, volatile components P_2O_5/SO_3, and iron oxides) [42] released gases through thermal decomposition or redox reactions at high temperatures, creating a porous structure within the ceramsite. Since the natural content of gas-generating components in solid waste was generally low, pore-forming agents often needed to be introduced to achieve effective expansion of the ceramsite.

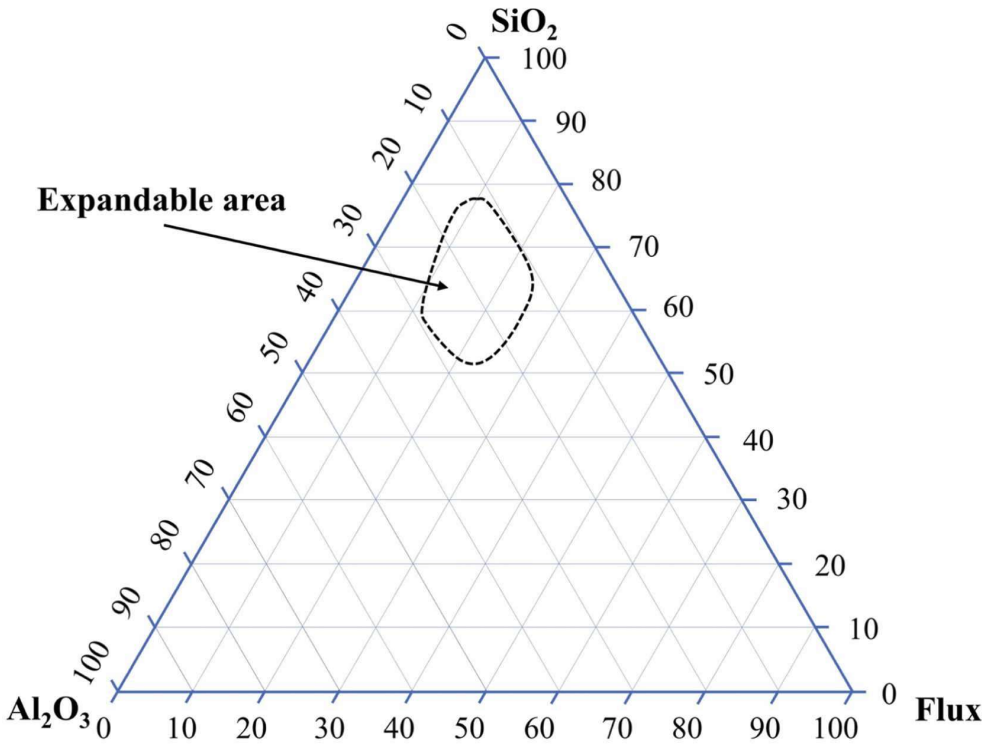

Figure 1. Range of chemical composition of suitable fired expanded ceramic pellets in the Riley ternary phase diagram (Reproduced from Ref. [43] with permission).

Table 1 systematically summarized the solid wastes commonly used in ceramsite production, revealing the following patterns and issues: The contents of major oxides (SiO_2, Al_2O_3, CaO, MgO, K_2O, Na_2O, and Fe_2O_3) varied significantly among different solid wastes, and their relative content was the key factor determining both the sintering behavior and final properties of the ceramsite. Since the chemical composition of a single solid waste generally failed to meet the ideal ratio requirements, it was often necessary to introduce another functionally complementary solid waste for component adjustment. Rational formulation design not only optimized the physical properties of the ceramsite but also significantly improved the comprehensive utilization efficiency of solid wastes. It was noteworthy that even for the same type of solid waste, significant chemical composition fluctuations existed due to differences in origin, treatment processes, and storage history, which posed challenges to process stability control during resource utilization. Furthermore, solid wastes often contained potentially hazardous components such as heavy metals, chlorine, and phosphorus. During ceramsite preparation, effective immobilization through methods like high-temperature sintering was required to ensure the environmental safety of the product.

Table 1. Different chemical components of solid waste.

Type of solid waste	Mass percent (%)									Ref.
	Loss of ignition	SiO_2	Al_2O_3	CaO	MgO	Fe_2O_3	K_2O	Na_2O	P_2O_5	
Phosphate tailing	2.90	66.52	16.76	0.35	0.78	1.40	3.92	0.08	0.16	[44]
Phosphate tailing	-	31.72	9.20	23.21	1.07	4.32	1.71	0.15	17.76	[45]
Phosphate tailing	7.21	59.12	26.01	2.34	2.91	1.45	3.87	0.35	-	[46]
Phosphate tailing	4.00	1.74	0.05	32.04	18.68	0.40	1.10	1.08	4.34	[47]
CRM	-	19.24	20.19	21.99	1.50	19.19	1.95	7.88	-	[48]
LSRM	-	6.73	43.75	11.8	-	19.76	1.52	8.62	-	[43]
Red mud	-	11.10	27.00	2.60	0.48	50.60	0.18	4.30	-	[49]
Red mud	-	20.40	27.80	3.02	-	28.50	0.12	13.90	0.20	[50]
DWTS	25.90	27.30	33.10	2.42	1.21	4.95	1.40	0.58	-	[51]
WWTS	50.00	12.01	7.87	2.95	0.87	5.16	1.34	0.31	-	[52]
Sewage sludge	-	39.19	9.12	4.86	2.06	22.05	-	-	-	[53]
MSWIFA	18.20	9.62	3.17	18.32	3.18	2.63	-	6.27	-	[54]
MSWI fly ash	-	2.50	0.77	64.32	0.69	-	4.74	3.81	-	[55]
MSWI fly ash	-	6.22	1.67	35.80	2.90	1.46	5.85	16.40	-	[56]
Iron tailings	-	44.87	12.07	11.32	6.28	14.97	0.67	2.69	-	[57]
Iron ore tailings	-	51.16	22.74	1.57	2.54	11.76	6.19	1.59	0.116	[58]
IOT	5.56	41.97	9.98	10.90	5.31	4.63	1.82	3.48	-	[59]
Fly ash	0.31	46.34	20.74	2.42	1.14	-	1.63	1.74	-	[60]
Coal fly ash	1.86	53.54	28.80	6.82	1.24	6.10	-	1.01	-	[61]
CFB fly ash	17.65	34.36	30.12	16.92	-	6.54	-	-	1.08	[62]
Fluorite tailings	-	64.81	13.70	3.85	1.86	-	2.68	1.77	-	[63]
Tungsten slag	-	8.39	2.65	6.54	0.19	8.71	0.12	0.08	-	[64]

2.1.2. Preparation methods

Based on the application of high-temperature thermal treatment, lightweight high-strength ceramsite was classified into sintered and non-sintered types. The manufacturing process of sintered ceramsite included raw material crushing, drying, mixing and formulation, pelletization, high-temperature sintering, and cooling. NSC (non-sintering ceramsite) utilized materials with pozzolanic activity as raw materials, which were crushed, dried, and mixed before an alkaline activator was incorporated to stimulate their reactivity [19,65], followed by pelletization and steam curing to form the final product. Formulation was the critical step in both processes, typically requiring the blending formulation of two or more solid wastes to adjust the chemical composition and meet performance requirements. For sintered ceramsite, the sintering process was the key stage determining critical properties such as water absorption, strength, and density, thereby influencing their suitable applications. This process was divided into preheating and sintering stages: the preheating stage removed moisture to prevent rapid gas release at high temperatures from causing

ceramsite cracking [66], while also creating a suitable reaction atmosphere for sintering; the sintering stage achieved microstructural formation and densification of the ceramsite through high-temperature reactions. For NSC, steam curing significantly enhanced mechanical strength by promoting pozzolanic reactions and hydration reactions [67].

Table 2 systematically summarized the key differences between the two main technical pathways for producing ceramsite from solid waste, namely the sintered and non-sintered methods, in terms of raw material formulation, process parameters, and product properties. Specifically, sintered ceramsite relied on solid wastes with high silicon and aluminum content as the main raw materials, and incorporated pore-forming agents (such as charcoal powder or SiC) to induce pore formation under high temperatures. Its process core was the preheating–sintering regime, aimed at achieving densification and microstructural control through physicochemical transformations at high temperatures (1100–1220 °C). In contrast, NSC utilized raw material systems with pozzolanic activity or cementitious potential (such as fly ash or slag) and depended on chemical activators (e.g., NaOH, CaO) to activate reactivity under ambient or low-temperature conditions. The key to its process lay in the control of curing conditions (temperature, humidity, and duration) to promote the geopolymerization or hydration reactions of cementitious phases. As a result, these fundamental differences led to significant distinctions in key properties such as water absorption, compressive strength, and bulk density, reflecting their distinct microstructural formation mechanisms based on high-temperature ceramification and ambient-temperature chemical bonding, respectively.

Table 2. Preparation techniques and characteristics of ceramsite derived from solid waste.

Types of ceramsite	Soild waste raw materials		Pore-forming agents (%)	Pyrolysis heating rate (℃·min^{-1})	Preheat		Pyrolysis		Physical and chemical properties of solid waste ceramisite			Ref.
Sintered ceramsite	Primary raw materials (%)	Auxiliary materials (%)			T (℃)	Time (min)	T (℃)	Time (min)	Water absorption (%)	Compressive strength (MPa)	Apparent density (Kg·m^{-3})[c]	
	Engineering excavated soil (75)	Fe_2O_3 powder (25)	Charcoal powder (2)	-	500	5	1150	5	5.3	5.02	1626.33	[20]
	Coal gangue (45)	Iron ore tailings (55)	-	-	-	-	1175	20	8.83	7.3	1756	[22]
	Fluorite tailings (70)	Clay (30)	SiC (0.5)	10	550	15	1210	30	0.02	4.63	890	[68]
	HCRM (50)	Dinas (40) Bentonite (10)	Industrial SiC (2)	-	500	5	1100	5	5.21	1.0	-	[66]
	Coal-fired fly ash:steel slag:gold tailings = 5:5:8		SiC (2) Corn straw (30)[a]	10, 15[b]	400	20	1170	10	0.22	15.6	1552.3	[69]
	Regolith granite sand washing sludge (60)	Silica fume (20) Red mud (20)	Phosphorus tailings (10)	10	450	20	1220	15	-	1.30	792.30	[70]
NSC	Raw materials (%)		Additives (%)		Curing temperature (°C)	Relative humidity (%)	Curing time (d)		WA (%)	CS (MPa)	AD (Kg·m^{-3})	
	Iron ore tailings:gangue:fly ash:cement:lime:gypsum = 35:10:28:15:10:2		NaOH (3) Aluminum powder (1)		80–85	99	2		17.6	2.27	-	[19]
	Sewage sludge:fly ash =8 :2		NaOH (9) CaO (6)		Room temperature	-	28		8.37	7.43	2603	[65]
	Water-washed IMSWA:ordinary Portland Cement: Silica Solt = 59:30:11		Aluminum powder		25	80	14		14	8	-	[71]
	River sediment:fly ash:slag:CaO:gypsum:sodium silicate = 70:15:10:2:2:1		40 wt% NaOH solution		20	65	7		5.3	6.4	-	[72]

Note: [a]: SiC was added at 0.2 wt% of the total raw material mass, while the addition of CS (corn straw) was chosen to be 30 wt% of the mass of Fe_2O_3 in the raw material. [b]: The staged regulation of heating rates was adopted to balance the stability of thermal behavior in the early stage and the efficiency of sintering in the later stage: a rate of 10 °C/min ensured adequate removal of moisture and organic matter, while 15 °C/min guaranteed thermal efficiency and phase transformation completeness during the sintering stage. [c]: The water absorption and apparent density of the ceramsite were determined in accordance with the Chinese national standard GB/T 17431.2-2010, and the compressive strength of individual ceramsite particles was measured using a computer-controlled electronic universal testing machine.

2.1.3. Energy consumption analysis

The investigation into ceramsite production remained largely confined to laboratory scale, with key energy-consuming steps including raw material crushing, granulation, drying, and sintering (or curing). For example, Ke et al. reported that the total energy consumption for producing 2.4 kg of ceramsite in a single batch was 77.1 kWh, of which sintering in a muffle furnace accounted for 40.55 kWh, representing 52.6% of the total [73]. Han et al. reported an energy consumption of 135 kWh per ton for NSC, with the curing stage alone consuming 96 kWh, contributing to 71.1% of the total [46]. Further analysis by Li et al. revealed that producing one ton of ceramsite required approximately 357.90 kWh in total energy, with sintering, drying, and preheating being the most energy-intensive stages, accounting for 35.70%, 29.34%, and 25.90% of the total consumption, respectively [74]. The aforementioned research results demonstrated that thermal treatment and curing represented the primary energy-consuming stages in ceramsite production. For sintered ceramsite, improving energy efficiency during the thermal treatment phase was crucial for reducing total energy consumption, achievable through adopting high-performance insulation materials, enhancing furnace heat recovery, and optimizing sintering protocols. For NSC, energy consumption was concentrated in the curing stage and could be effectively controlled by optimizing curing regimes and utilizing chemical activators. Advancing the transition from laboratory-scale preparation to scaled-up, continuous production, along with implementing intelligent process control systems, systematically enhanced energy utilization efficiency and provided key technical support for the green manufacturing and broad application of ceramsite.

2.1.4. Carbon footprint analysis

Carbon footprint served as a key indicator for quantifying the total greenhouse gas emissions of ceramsite throughout its entire life cycle (Figure 2). Systematic assessment of it is of great significance for promoting the green manufacturing and sustainable development of solid waste-based ceramsite. Existing studies generally adopted the life cycle assessment method, with system boundaries typically covering stages such as raw material acquisition, production processing, transportation, use, and waste disposal. For example, Song et al. compared the carbon footprints of three types of solid waste-based ceramsite made from sewage sludge, fly ash, and sludge-aluminum ash, with values of 0.93, 0.69, and 0.66 kg CO_{2eq}, respectively. The production stage contributed to over 80% of the total emissions, highlighting its dominant role in the overall carbon footprint [75]. In a more detailed analysis, Li et al. divided the ceramsite production process into four stages: raw material production, transportation, manufacturing, and product dispatch. Their findings revealed that raw material production accounted for only 11.47% of the total emissions, while the drying and

sintering stages contributed 20.73% and 63.07%, respectively, collectively constituting the primary emission sources [76]. Similarly, the calculation by Han et al. indicated that the carbon emission per ton of ceramsite produced was 121.69 kg CO_2, with the production process accounting for 65.0% of the total, further underscoring energy-intensive processes as key contributors to carbon emissions [46]. Furthermore, Gao et al. utilized construction waste soil to produce non-sintered lightweight aggregates, with carbon emissions ranging from 47.40 to 201.17 kg CO_2/t. Through systematic comparison, they demonstrated that this process could reduce the global warming potential by 31% to 84% compared to conventional landfill disposal, highlighting the significant carbon reduction potential of the solid waste recycling approach [77].

Future carbon emission reduction in ceramsite products requires a multi-path synergistic system, where the transition to a cleaner energy infrastructure, enhanced process efficiency, and optimized industrial chains jointly promoted the utilization of solid waste and the development of low-carbon building materials.

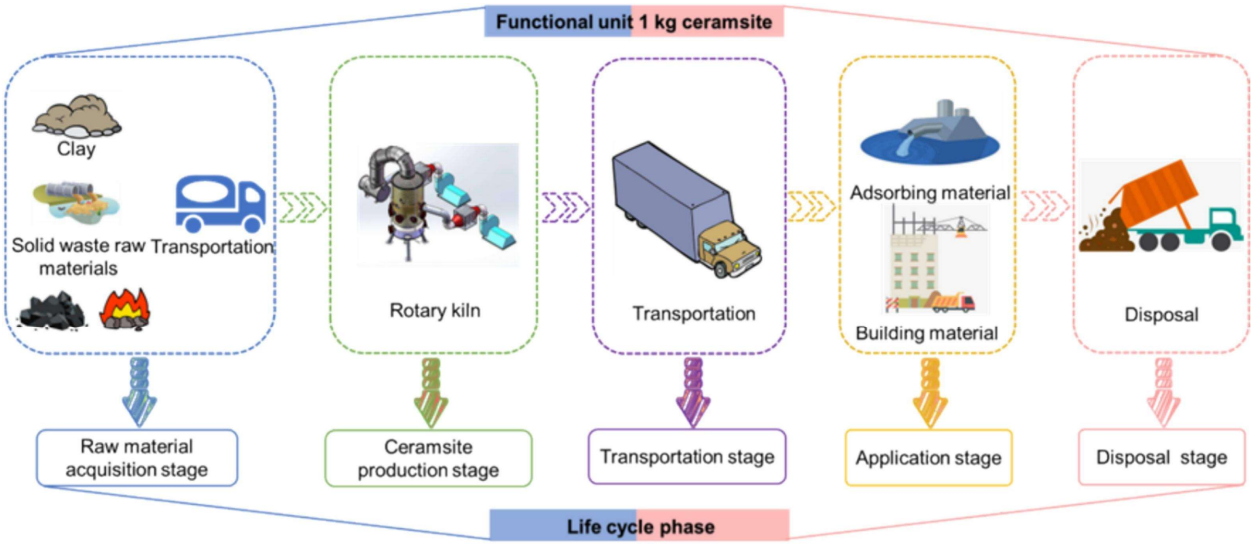

Figure 2. System boundary for the life cycle carbon footprint analysis of ceramsite (Reproduced from Ref. [75] with permission).

2.1.5. Comparison between solid waste-based ceramsite and natural ceramsite

Solid waste-based ceramsite exhibited significant advantages over natural lightweight aggregate in terms of raw material characteristics, thermal efficiency, and environmental benefits. Regarding raw materials, the organic carbon and volatile components in solid waste-based ceramsite served as auxiliary fuels during sintering, reducing reliance on external fossil fuels. In contrast, natural lightweight aggregate, with its homogeneous composition, lacked self-supplying fuel capacity and depended entirely on external energy input. In thermal processes, although solid waste raw materials showed compositional fluctuations, multi-component blending and precise temperature control, combined with heat release from inherent combustible components, enhanced overall thermal efficiency. While natural aggregate demonstrated consistent composition and stable processing, its lack of endogenous energy supplementation resulted in a lower overall system efficiency ceiling. For waste heat utilization, the multi-stage high-temperature processes in solid waste-based ceramsite

production generated concentrated and substantial waste heat, enabling the establishment of efficient heat recovery systems for cascaded energy utilization. Natural aggregate processing, being simpler with fewer high-temperature stages, offered limited waste heat recovery potential. From a life cycle perspective, solid waste-based ceramsite eliminated the need for mineral mining and primary crushing, substantially reducing preliminary energy consumption and ecological disturbance while achieving waste valorization. Combined with the utilization of inherent combustibles and waste heat recovery, its carbon footprint was significantly lower than that of natural aggregate, demonstrating superior synergy between environmental protection and energy efficiency.

2.2. Key factors influencing the performance of solid waste-based ceramsite

2.2.1. Proportion of raw materials

For sintered ceramsite, the raw material ratio governed the phase evolution and microstructure development during sintering by altering the Si/Al ratio and the silica-alumina content, thereby determining its final properties. The raw material formulation determined the performance of ceramsite by governing the phase evolution and structural development during sintering through adjustments in the Si/Al ratio and the total SA (SiO_2 and Al_2O_3) content. A high Si/Al ratio, particularly when coupled with an increase in network modifiers, promoted the formation of abundant low-viscosity liquid phase [40]. This liquid phase effectively encapsulated gas bubbles to create pores, which drove the expansion of ceramsite and reduced its apparent density; concurrently, it filled surface pores, thereby lowering the water absorption of ceramsite. Conversely, a low Si/Al ratio favored the crystallization of strength-enhancing phases such as mullite, which directly improved the strength of ceramsite by reinforcing its crystalline framework. An excessively low total SA content resulted in an insufficient liquid phase, leading to densification shrinkage, an increase in density, and strength degradation due to poor particle bonding. In contrast, an excessively high SA content caused over-fusion, resulting in softening and deformation of the ceramsite. Only a moderate SA content facilitated the formation of an adequate liquid phase to promote sintering while ensuring sufficient crystallization of mullite, thereby achieving optimal strength [78–80]. According to the study by Liu et al., an increase in the Si–Al ratio of the raw materials led to the generation of a greater amount of liquid phase with reduced viscosity during the sintering of ceramsite. This change promoted the expansion of ceramsite, resulting in a decrease in AD and CS. Meanwhile, the escape of a small amount of gas from the low-viscosity liquid phase created some open pores, which caused a slight increase in WA [37]. According to the study by Zheng et al., when the content of clay (with 28.35% Al_2O_3) in the raw materials was low, it led to a weakened, porous, and inadequately consolidated structure in the ceramsite, resulting in decreased compressive strength and increased water absorption [53]. According to the study by Zhang et al., when the content of sludge (with 28.35% SiO_2) in the raw materials was excessively high, the increased liquid phase and the release of gases led to denser ceramsite. However, over-firing resulted in an incomplete internal structure, making it prone to noticeable collapse and cracking, which significantly reduced the strength of the ceramsite [81]. For NSC, raw material systems typically utilized solid wastes with pozzolanic activity or cementitious potential, supplemented with cement as an additional binder. These components reacted during hydration to form C-S-H gel, thereby enhancing the strength of the ceramsite. In the design of the raw material mix, the properties and proportions of each component directly influenced the

microstructure and pore characteristics of the ceramsite, which in turn determined its density and water absorption. For instance, Xu et al. found that as the OPC (ordinary portland cement) content increased, the loose bulk density of the ceramsite initially rose and then declined, while the compressive strength continuously improved [71]. Similarly, Liu et al. demonstrated that with an increase in blast furnace slag content, both the compressive strength and compactness of the ceramsite increased, whereas the water absorption decreased significantly. This was attributed to the active components in the slag participating in hydration reactions, which effectively filled pores and refined the pore structure, thereby enhancing the densification of the system [82].

2.2.2. Additives

In the preparation of ceramsite, additives referred to functional substances incorporated to regulate or optimize their physicochemical properties. Based on their mechanisms of action, they were categorized into pore-forming agents and activators. For sintered ceramsite, pore-forming agents generated gases through chemical reactions or physical decomposition during high-temperature sintering, thereby forming uniformly distributed pore structures within the ceramsite and reducing its density. Commonly used pore-forming agents included carbon powder (carbon powder participated in a redox reaction with Fe_2O_3, resulting in gas generation, as shown in Eqs 1–4. It also reacted with O_2 and CO_2 to produce gas, as indicated in Eqs 5 and 6), Fe_2O_3 (as shown in Eq 7), SiC (as shown in Eq 8), and solid wastes rich in carbon or volatile components (as shown in Eqs 9 and 10). For example, Sun et al. used CS (corn straw) and SiC as expanding agents in their study and found that, compared to CS, SiC exhibited better gas generation, resulting in a more developed pore structure [69]. Zhan et al. utilized SAD (secondary aluminum dross) as a foaming agent to produce lightweight ceramsite, where the AlN contained in SAD underwent oxidative decomposition at high temperatures, releasing N_2 (as shown in Eq 11) and promoting the expansion of the foamed glass-ceramics [83]. Xiao et al. successfully prepared ultra-lightweight ceramsite using phosphate tailings as a foaming agent, in which dolomite and calcite decomposed at high temperatures to release CO_2, effectively facilitating pore development and volume expansion [70]. Current research demonstrated that employing solid wastes as pore-forming agents not only contributed to the lightweight and functionalization of ceramsite but also provided a feasible pathway for developing environmentally friendly ultra-lightweight building materials, offering both environmental and economic benefits. In the preparation of NSC, activators promoted the dissolution and polymerization of active SiO_2 and Al_2O_3 in the raw materials through an activation mechanism, forming a cementitious matrix with a three-dimensional network structure. This gel network interlocked and bound the raw material particles together at the microscopic level, while also optimizing the internal pore structure. Macroscopically, this structural transformation directly resulted in improved compressive strength and influenced the bulk density and water absorption of the ceramsite. For example, Wang et al. used NaOH as an activator to prepare ceramsite green pellets and found that as the NaOH concentration increased, the compressive strength of the green pellets also rose, reaching a maximum value of 12.34 MPa [57]. Chen et al. used QL (quicklime powder), NaOH, and SS (sodium silicate solution) as composite alkali activators to prepare ceramsite and found that NaOH not only enhanced the early-age strength contribution of QL but also worked synergistically with SS to promote sustained strength development, effectively compensating for the limitations of QL alone in strength development [84]. Similarly, Xu et al. employed a ternary activation system composed of cement,

quicklime, and gypsum, and observed that the synergistic effect of the three significantly increased the variety and quantity of hydration products. This system promoted hydration and carbonation reactions within the cementitious materials, thereby regulating the formation of the microstructure and holistically optimizing the physical and mechanical properties of the ceramsite [85].

$$2Fe_2O_3 + C \rightarrow 4FeO + CO_2 \quad (1)$$

$$2Fe_2O_3 + 3C \rightarrow 4Fe + 3CO_2 \quad (2)$$

$$Fe_2O_3 + C \rightarrow 2FeO + CO \quad (3)$$

$$Fe_2O_3 + 3C \rightarrow 2FeO + 3CO \quad (4)$$

$$C + CO_2 \rightarrow 2CO \quad (5)$$

$$3C + O_2 \rightarrow 2CO + CO_2 \quad (6)$$

$$2Fe_2O_3 \rightarrow 4FeO + O_2 \quad (7)$$

$$SiC + 2O_2 \rightarrow CO_2 + SiO_2 \quad (8)$$

$$CaCO_3 \rightarrow CaO + CO_2 \quad (9)$$

$$CaMg(CO_3)_2 \rightarrow CaO + MgO + 2CO_2 \quad (10)$$

$$4AlN + 3O_2 \rightarrow 2Al_2O_3 + 2N_2 \quad (11)$$

2.2.3. Curing process

In the ceramsite preparation process, curing refers to the critical process step that transformed loose ceramsite green pellets into stable particles with specific mechanical strength. Sintered ceramsite employed thermal curing, while NSC relied on chemical curing.

In the preparation of sintered ceramsite, the thermal curing regime served as a critical process step, primarily involving parameters such as preheating temperature, preheating time, sintering temperature, and sintering duration. The preheating stage was designed to effectively remove volatile components from the raw materials, preventing the violent release of gases during subsequent high-temperature sintering that could cause structural damage, thereby creating a stable reaction environment for the sintering process. For example, J. Manosa pointed out that insufficient preheating led to the rapid decomposition of volatile components in aggregates rich in waste sludge during sintering, releasing large volumes of gas that caused the brittle external structure of the ceramsite to crack, significantly compromising the integrity of the final product [86]. Preheating temperature and time had a notable impact on the final properties of the ceramsite. For instance, Shen et al. further observed that as the preheating temperature increased, the pellet strength and density of the ceramsite initially decreased and then increased, while water absorption first rose and then fell. Under a fixed preheating temperature, prolonging the preheating time resulted in an initial increase followed by a decrease in strength and density, whereas water absorption first decreased and then increased [44]. Liu et al. demonstrated that as the preheating temperature increased, the compressive strength of the ceramsite improved accordingly; however, when the temperature exceeded 400 °C, the strength began to decline. Meanwhile, extending the preheating time promoted strength development and reduced water absorption [64].

In the preparation of sintered ceramsite (Figure 3), sintering temperature and sintering time served as critical control parameters that collectively determined the final properties of the ceramsite. When the sintering temperature fell below the melting threshold of the raw material system, the generated molten phase failed to fully encapsulate the raw material particles, and the decomposition rate of gas-producing substances was lower than the diffusion rate. As a result, neither sufficient internal gas pressure to support expansion nor a continuous molten network could be established. Under such conditions, two scenarios could occur: first, the ceramsite remained unsintered and unexpanded, exhibiting low strength and density; second, although partially sintered, it did not expand, resulting in improved strength but still substandard density, along with significantly high water absorption due to the lack of an effective surface glaze layer. When the sintering temperature was excessively high, an overabundance of molten phase was generated, leading to excessive filling of pores and over-densification of the structure. In severe cases, particle deformation or collapse occurred due to gravitational effects. Under these conditions, while the ceramsite might exhibit high strength, its density was too high, water absorption too low, and shape difficult to control, contradicting the goal of lightweight performance. When the sintering temperature remained within the appropriate range, a dynamic balance was achieved between the amount of molten liquid phase generated and the gas release rate. On one hand, the liquid phase sufficiently encapsulated the particles and formed a dense surface glaze layer, effectively trapping the escaping gases. On the other hand, moderate gas pressure created a uniform closed-pore structure within the viscous melt. Macroscopically, this was reflected as increased strength, moderate density, and reduced water absorption, achieving synergistic optimization of structure and performance. When the sintering time was too short, insufficient solid-state reactions and liquid phase formation prevented the effective development and expansion of gases, resulting in a loose ceramsite structure with low strength and increased water absorption due to the presence of open pores. When the sintering time was too long, exceeding the optimal duration for the raw materials, continuous liquid phase formation filled and sealed pores, leading to excessive densification and even particle softening and deformation. This process not only increased energy consumption but also caused a rise and subsequent decline in strength, overly low water absorption, and over-sintering. When the sintering time was appropriate, solid-state reactions proceeded sufficiently, and the liquid phase developed within a suitable range. Particles bonded densely through cohesion, while internally generated gases promoted uniform expansion of the ceramsite. Under these conditions, the ceramsite exhibited significantly enhanced strength, reasonably controlled density, and effectively reduced water absorption, achieving an optimal balance in performance.

Sun et al. found that a solid-state reaction between CaO and SiO_2 during sintering generated a high-strength and thermally stable wollastonite phase, which effectively enhanced the macroscopic strength of the ceramsite. However, when the sintering temperature increased to 1090 °C, the wollastonite content decreased, resulting in a reduction of the ceramsite strength. Simultaneously, the decomposition of calcite in the raw material released CO_2 gas, which became trapped in the molten glass phase, forming numerous discrete micropores and thereby significantly reducing the apparent density of the ceramsite [48]. Xiao et al. found that increasing the calcination temperature caused phosphogypsum in the ceramsite to decompose, generating SO_2. This gas decreased the surface tension of the melt, leading to thinning or even collapse of the pore walls, thus weakening the overall strength of the ceramsite. However, with prolonged sintering duration, the amount of liquid phase on the ceramsite surface gradually increased. The surface tension of the liquid phase caused solid

particles to move closer together, while the liquid phase further penetrated into the pores, effectively promoting the densification process and thereby enhancing the strength of the ceramsite [87]. Luo et al. observed that when the temperature reached 950 °C, the glass phase reaction in the system approached completion, manifested as a significant weakening of quartz diffraction peaks alongside enhanced intensities of anorthite and mullite diffraction peaks. This phase transformation promoted the formation of a Ca-Si-Al-based structural skeleton within the ceramsite, thereby effectively enhancing its mechanical strength and structural stability [88]. Li et al. found that when the temperature increased to 1200 °C, CaO, SiO_2, and Al_2O_3 in the raw materials reacted to form crystalline phases such as quartz, anorthite, and mullite. However, as the temperature continued to rise, the diffraction intensities of all crystalline phases except quartz significantly weakened, leading to a decrease in the overall strength of the ceramsite. Simultaneously, the elevated temperature promoted the formation of a liquid phase on the ceramsite surface, which hindered the escape of internally generated gases and ultimately caused volume expansion [89].

Figure 3. Effect of the sintering temperature and duration on the surface morphology of ceramsite (Reproduced from Ref. [69] with permission).

In the preparation of NSC, chemical curing was a critical step, with key conditions including temperature, humidity, and curing duration, which collectively determined the final properties of the ceramsite. The underlying mechanism lay in the direct influence of these parameters on the hydration process of cementitious materials (such as cement and fly ash) as well as on the composition and structure of hydration products (Figure 4). Specifically, temperature served as a key variable significantly influencing the kinetics of the hydration reaction: suitable temperatures accelerated the hydration process and promoted the formation of more hydration products like C-S-H gel; excessively low temperatures markedly slowed the reaction, leading to delayed early-age strength development; while overly high temperatures caused premature moisture evaporation, resulting in incomplete hydration. Humidity conditions determined the state of the reaction medium and played a crucial role in both the continuity of hydration and the evolution of the pore structure: under saturated humidity conditions, the hydration reaction proceeded sufficiently, and the resulting

hydration products effectively filled interparticle voids, thereby optimizing the pore structure, reducing total porosity, and decreasing the proportion of large pores. The curing period provided the necessary time for the aforementioned hydration reactions and microstructural evolution, ensuring that the desired degree of hydration was achieved and facilitating the stabilization of the microstructure and the development of properties [90]. Ding et al. found that under a curing condition of RH (relative humidity) ≥95%, the addition of an activator could provide sufficient OH^- and $[SiO_4]^{4-}$, which rapidly reacted with Ca^{2+} and Al^{3+} to form C-A-S-H gel; the prepared ceramsite exhibited a cylinder compressive strength of 7.43 MPa [91]. Shahane et al. found that increasing the curing temperature of fly ash ceramsite from 65 to 75 °C resulted in an increase in compressive strength from 15 to 18 MPa [92]. Cao et al. found that when the curing duration was extended from 14 to 20 d, the bulk density of the ceramsite increased from 750 to 860 kg/m^3; this was attributed to the substantial participation of moisture and gases from the air, which led to the ongoing hydration process [93].

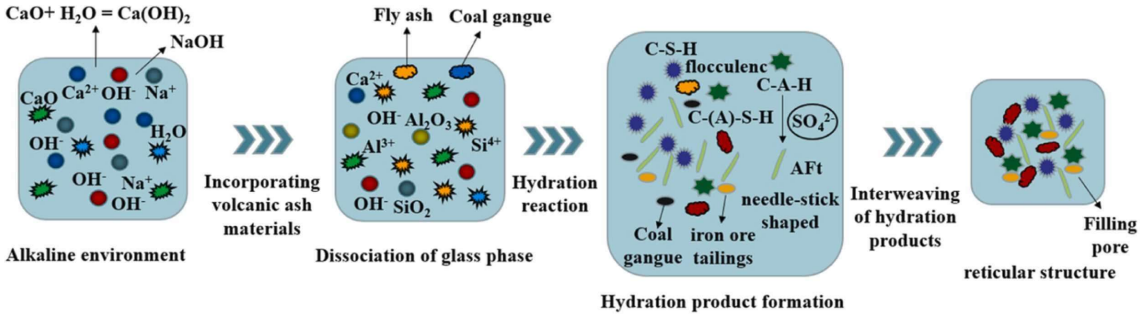

Figure. 4. Alkali-excited ceramsite hydration mechanism diagram (Reproduced from Ref. [19] with permission).

2.3. Curing mechanisms in solid waste-based ceramsite

Current research on the ceramsite curing mechanism primarily focused on key microscopic processes, including phase evolution, structural formation, and morphological development. To systematically reveal the intrinsic mechanisms during ceramsite curing, this chapter analyzed the topic from three aspects: phase changes, structural formation, and mass transfer processes, with separate discussions on the curing mechanisms for both sintered and non-sintered ceramsite.

2.3.1. Physical phase changes

During the sintering process of ceramsite, Al_2O_3 and SiO_2 underwent transformation and reorganization, forming a three-dimensional network skeleton structure primarily composed of Si-O-Si and Si-O-Al bonds, which provided fundamental structural support for the ceramsite. As the thermal reaction proceeded, components with poor thermal stability in the system were progressively transformed into more thermally stable mineral phases, generating various thermochemical products such as molten glass phase, mullite, feldspar phase, and pyroxene phase. These thermochemical products played distinct key roles at the microstructural level, collectively establishing the foundation for the macro-properties of the ceramsite. The molten glass phase acted as a high-temperature binding medium, not only facilitating mass transfer and reactions between particles through its

fluidity but also effectively bonding crystal grains upon cooling, significantly enhancing the overall structural compactness and interparticle bonding strength [94,95]. Mullite, with its excellent high-temperature stability and interwoven acicular crystal morphology, markedly improved the mechanical strength and creep resistance of the ceramsite [96]. The feldspar phase primarily served a filling and connecting role in the structure, contributing to the optimization of the phase composition and enhancing the overall thermal stability. The pyroxene phase exhibited a significant capacity for immobilizing heavy metal ions, stabilizing them within the crystal lattice and thereby reducing environmental risks. Additionally, other phases such as spinel phases could form in the system, further improving the high-temperature performance and chemical durability of the material. Through synergistic action at high temperatures, these thermochemical products collectively endowed the sintered ceramsite with excellent mechanical properties, thermal stability, and environmental safety. Zhang et al. found that with increasing temperature, new phases including albite, bytownite and anorthite formed during the sintering process, generating multiple silicate liquid phases that enhanced the bonding structure of the ceramsite and consequently improved its strength [81]. Li et al. studied the X-ray diffraction (XRD) patterns of ceramsites calcined at different temperatures and found that with increasing temperature, the crystal transformation of quartz into cristobalite constituted the ceramic skeleton, thereby enhancing the strength of the ceramsites [97]. Li et al. found that introducing an appropriate amount of SiC as a pore-forming agent during ceramsite preparation achieved dual functions of pore creation and matrix enhancement through the high-temperature oxidation reaction (Figure 5). CO_2 generated pores to achieve lightweight, while the resulting SiO_2 acted as an active silicon source promoting the formation of a glass phase and high-strength crystalline phases such as mullite. This compensated for strength loss while increasing porosity, leading to synergistic optimization of material properties. However, excessive SiC addition caused uncontrolled pore expansion, which compromised structural integrity and increased raw material cost [76,98,99]. Xu et al. found that when the sintering temperature exceeded 1100 ℃, the diffraction peak intensity of kyanite phase significantly increased while those of albite and diopside continued to rise, resulting in a system dominated by feldspar and pyroxene phases. The interwoven and intergrown microstructure thus markedly enhanced the compressive strength of the ceramsite [100].

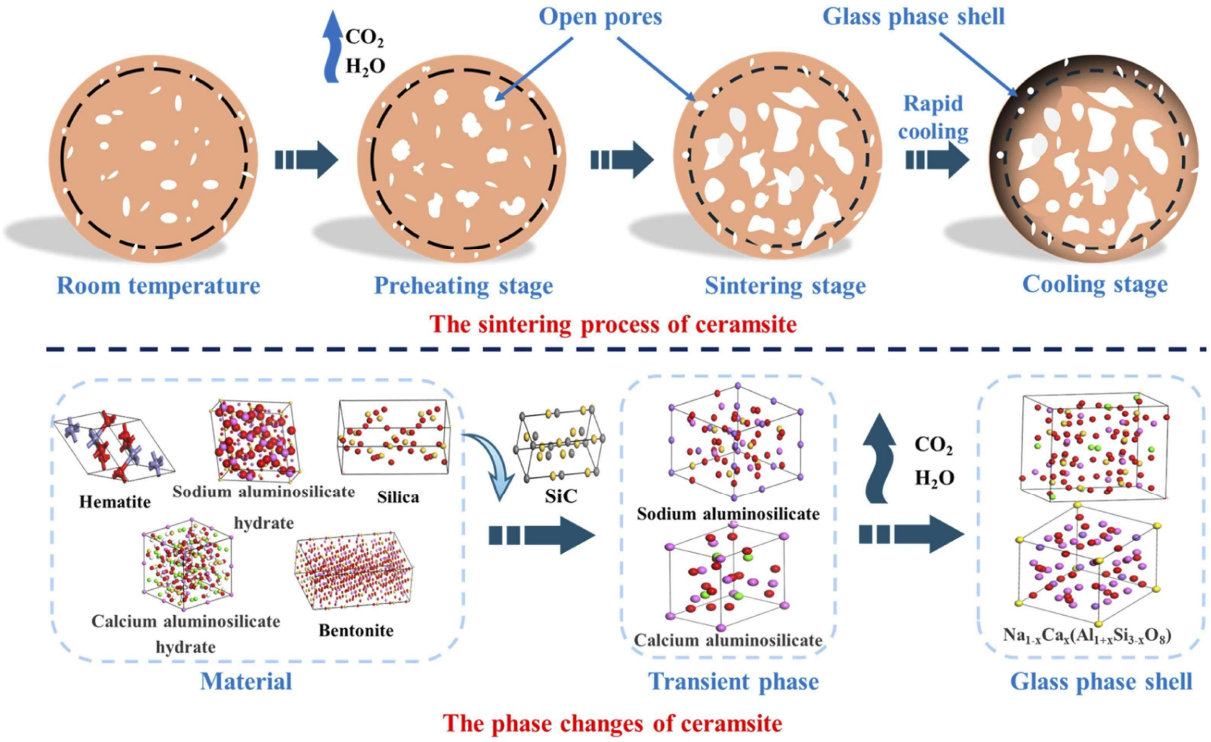

Figure 5. Expansion mechanism diagram of ceramsite (Reproduced from Ref. [66] with permission).

2.3.2. Structural formation

The structural formation of ceramsite involved surface densification and the development of an internal pore structure. Riley pointed out that two fundamental conditions needed to be simultaneously satisfied for the expansion of raw materials during high-temperature sintering: a high-viscosity glass phase and sufficient gas-generating substances [33]. This was because the gas produced by gas-generating substances served as the basis for pore formation, with the number of pores directly influencing the degree of expansion of the ceramsite; meanwhile, the viscosity of the glass phase regulated the morphology and distribution of the pores: the more uniform the pores, the higher the internal structural strength of the ceramsite. As the calcination temperature increased, the proportion of the liquid phase in the system gradually rose, while its viscosity correspondingly decreased. It was noteworthy that an excessively high liquid phase viscosity hindered gas expansion and pore formation, whereas an overly low viscosity failed to effectively encapsulate the gas, leading to pore coarsening or collapse. Ideal structural formation relied on a dynamic balance between gas pressure and liquid phase viscosity; when the two approached equilibrium, a uniformly distributed pore structure could form inside the ceramsite. During the sintering process, the surface of the ceramsite heated at a faster rate than the interior, leading to the initial formation of a molten phase that was greater in quantity and higher in fluidity compared to that inside. The foaming behavior in the surface region became covered as the molten phase developed and its fluidity increased, thereby promoting the progression of the surface layer toward densification. Simultaneously, in the high-temperature environment inside the ceramsite, gas was captured and immobilized by the high-viscosity molten glass phase, forming pores through foaming. The extensive development and

distribution characteristics of these pores collectively constructed the internal pore structure of the ceramsite, whose abundance and morphological features directly determined the physical properties and application characteristics of the ceramsite.

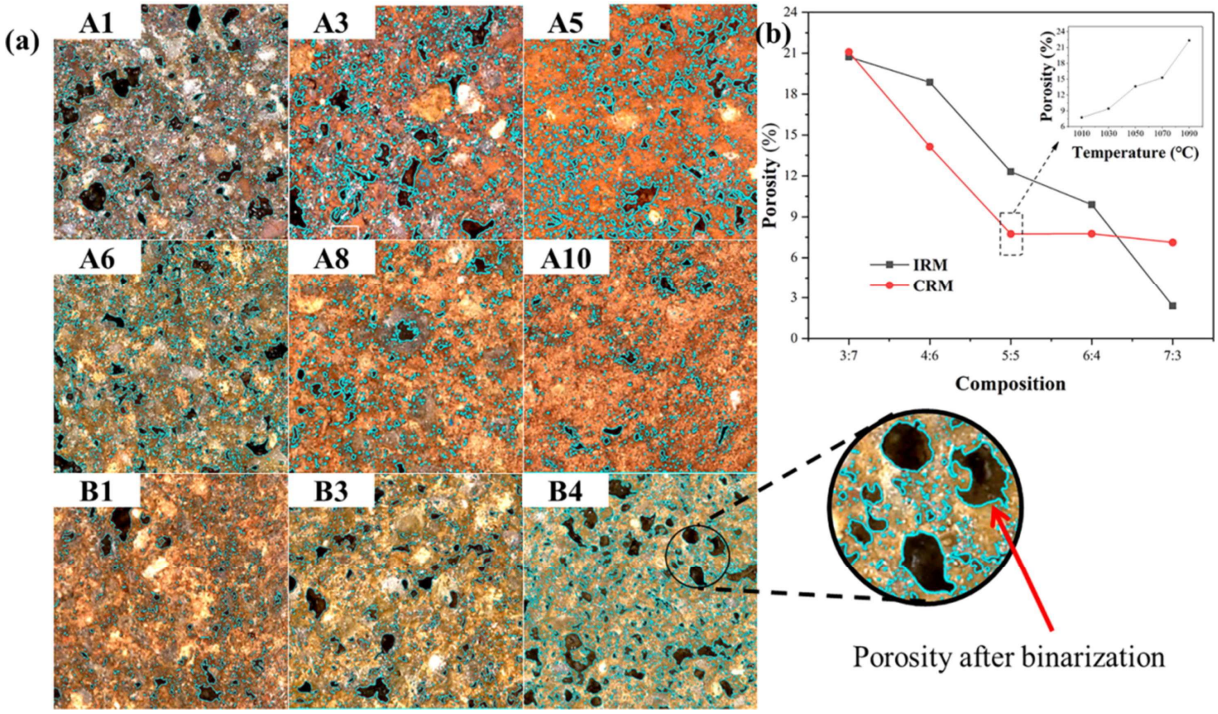

Figure 6. (a) Cross-sectional images of different ceramsites with a magnification of 40 times, and (b) porosity values of ceramsites produced from different proportions of materials and firing temperatures (Reproduced from Ref. [48] with permission).

Sun et al. conducted studies on the structure formation of ceramsite. Their analysis of the ceramsite microstructure revealed that the pores primarily originated from the CO_2 gas released by the thermal decomposition of calcite, which formed a gaseous pore structure. However, with the increase in red mud (RM) content, the interfacial porosity of the ceramsite significantly decreased, leading to an increased degree of densification. This structural change was unfavorable for the development of lightweight properties in the ceramsite. The images in Figure 6, which depict the cross-sectional views of the ceramsite, were binarized and marked with blue lines to indicate the location and size of holes. Mi et al. observed through Scanning electron microscopy (SEM) analysis that the thermal decomposition of calcite and other components in the raw materials generated numerous micropores, most of which were subsequently filled by the liquid phase. This structure significantly enhanced the compressive strength of the ceramsites and effectively hindered the leaching of hazardous substances [80]. Qin et al. compared SEM images of ceramsites with different additives and found that samples with sawdust formed the largest pores due to organic matter combustion, resulting in the highest water absorption and apparent porosity, but the lowest cylinder compressive strength [61]. Wu et al. systematically studied the effect of MSWI (Municipal solid waste incineration fly ash) content on the microstructure of ceramsites and found that when the content was below 20 wt%, the ceramsites exhibited appropriately distributed pores, mostly filled by the liquid phase, which helped reduce water absorption. However, with further increase in MSWI fly

ash content, the pores expanded and interconnected into larger cavities, adversely affecting both the compressive strength and water absorption resistance of the ceramsites [55]. Pei et al. conducted Fourier-transform infrared spectroscopy (FTIR) spectral analysis on NEC (non-expanded clay) and found that the peak at 536 cm^{-1} indicated the presence of a Si-O-Al structure, which contributes to the strength of ceramsite.

2.3.3. Mass transfer

According to G. C. Kuczynski's sintering theory, powder particles undergo mass transfer and material migration during high-temperature calcination, leading to interparticle contact, a reduction in the specific surface area, and ultimately resulting in particle bonding and densification. In the ceramsite sintering process, this mechanism manifested as two distinct pathways: surface mass transfer and internal mass transfer. The molten glass phase formed under high temperature not only provided the driving force for viscous flow mass transfer, facilitating bulk material migration, but also created conditions for dissolution-precipitation mass transfer through the liquid phase. Surface mass transfer occurred primarily on the hotter surface of the ceramsite [101], where liquid phase flow filled surface pores and formed an aluminosilicate coating, effectively blocking the migration of reactive components and thereby significantly reducing the leaching risk of hazardous substances. The internal mass transfer process was more complex: on one hand, under capillary forces, unsintered fine particles, alkali metals, heavy metals, and other components underwent viscous flow through the glass phase; on the other hand, these substances (especially soluble components) dissolved into the molten glass phase and subsequently reprecipitated and crystallized on the surfaces of larger particles due to supersaturation. These dissolution-precipitation processes, together with material migration, collectively promoted particle coalescence and overall structural densification, thereby endowing the ceramsite with enhanced mechanical strength and chemical stability at the macroscopic level.

According to multiple studies, mass transfer during ceramsite sintering directly governed the evolution of its internal structure and ultimately dictated its macroscopic properties. For instance, Sun et al. observed that RM particles and fine MSWI bottom ash particles migrated into larger MSWI bottom ash particles under capillary forces and crystallized there, which directly contributed to the construction and strengthening of the internal framework of the ceramsite [48]. Li et al. found that the liquid phase formed by rapid melting on the ceramsite surface not only promoted particle rearrangement and densification through viscous flow but also drove the migration of alkaline metal oxides toward the interior, thereby reducing the instability caused by alkali enrichment on the surface [102]. The comprehensive analysis by Mi et al. further revealed that the aluminosilicate framework formed during mass transfer effectively encapsulated heavy metals, while SEM results confirmed that liquid phase filling pores significantly optimized the pore structure (Figure 7). Pei et al. observed through SEM examination of the ceramsite microstructure that mass transfer of liquid phase with sufficient viscosity captured gases, forming semi-enclosed spherical pores, which contributed to the reduction of water absorption [103].

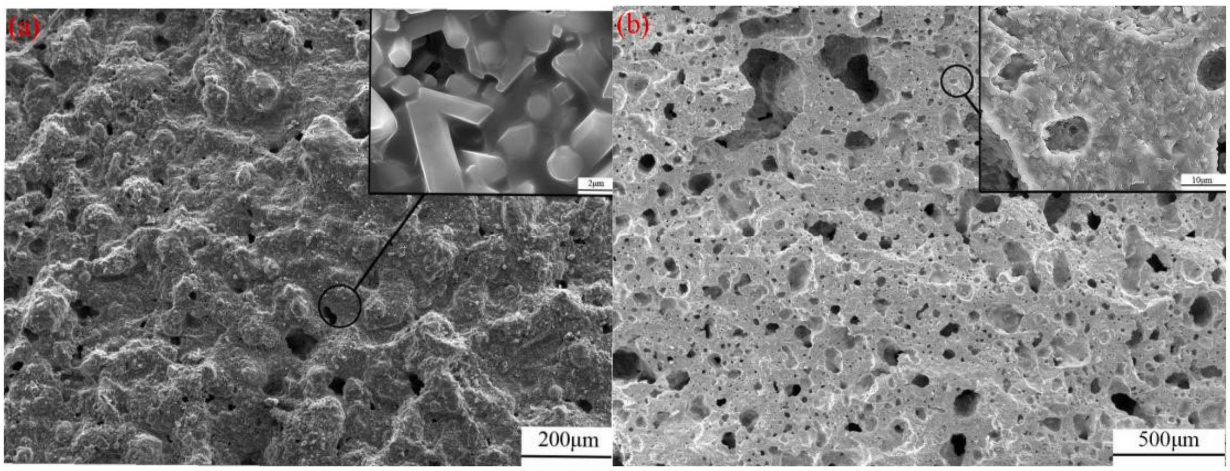

Figure 7. SEM images of (a) outer surface and (b) cross section of ceramsite prepared under optimum synthetic conditions (Reproduced from Ref. [80] with permission).

3. Application of solid waste-based ceramsite in lightweight concrete

3.1. Building materials

Due to its low density, high strength, low thermal conductivity, and good fire and heat resistance, ceramsite was widely used as a lightweight aggregate to produce LWHSC. This type of concrete exhibited excellent performance in strength, density, and thermal insulation, making it particularly suitable for fields requiring high comprehensive performance requirements.

The primary application lay in structural self-insulation and energy conservation. Ceramsite was characterized by low thermal conductivity and good heat resistance. Lightweight concrete prepared using ceramsite as aggregate served as thermal insulation wall material. It functioned by inhibiting heat exchange between the interior and exterior to regulate indoor temperature, thereby achieving building energy efficiency. For instance, foam concrete prepared by Wang et al. using ceramsite as aggregate exhibited excellent compressive performance and primarily played a role in absorbing energy for structural protection [104]. Wang et al. developed a concrete using paraffin-impregnated ceramsite as aggregate, which exhibited remarkable energy storage and thermal regulation capabilities, making it highly suitable for building thermal management [105]. The heat-storage concrete developed by Li et al., which incorporates phase-change ceramsite sand as aggregate, exhibited promising potential for energy conservation and renewable energy utilization [106]. The foamed concrete laminated composite floor slabs prepared by Liu et al., utilizing ceramsite as aggregate, exhibit the characteristics of being lightweight and excellent thermal insulation performance, rendering them suitable for thermal insulation purposes [107]. The thermal insulation concrete was prepared by Wang et al., utilizing ceramsite as the aggregate. They investigated the impact of sand ratio and sandwich layer thickness in composite wall panels on its thermal conductivity, demonstrating its potential as a viable material for thermal insulation purposes [108]. Zeng et al. utilized composite ceramsite as an aggregate in the production of concrete blocks and employed it as the primary building material for energy-efficient self-insulated exterior wall enclosures, achieving a 50% reduction in energy consumption compared to target requirements [109].

Li et al. utilized ceramsite derived from paper sludge as an aggregate to fabricate lightweight concrete for application in self-insulated walls, demonstrating its compliance with the design standards for energy conservation in residential buildings located in regions with severe cold and cold climates (JGJ26-2018) [110].

Secondly, lightweight high-strength ceramsite was applied in both the renovation of existing buildings and new construction, owing to its low density and the excellent workability of the resulting concrete. The lightweight concrete prepared with it significantly reduced structural load, thereby enabling renovations without imposing additional load on the original foundation and markedly improving the overall performance of the renovated sections. For instance, Zhu et al. produced all-lightweight ceramsite concrete using ceramsite as aggregate and applied it as a repair material for ordinary concrete. Through splitting tensile tests, they systematically investigated the interfacial tensile performance between the two types of concrete, demonstrating the feasibility of using lightweight concrete as a repair material [111]. Zhou et al. employed ceramsite as the aggregate for fabricating lightweight concrete, thereby effectively addressing the challenges associated with adding floors and extracting columns during the reinforcement and renovation of existing buildings [112].

The subsequent application was in precast components. Owing to its comprehensive advantages of low self-weight, high strength, and excellent workability, ceramsite was used as a lightweight aggregate to produce concrete that was well-suited for the industrial production of precast elements. Consequently, this type of lightweight concrete was widely employed in manufacturing various load-bearing and non-load-bearing precast members. For example, Sun et al. mixed high-titanium heavy slag with different types of ceramsite and used them as aggregates to produce lightweight ceramsite high-titanium heavy slag concrete for prefabricated composite panels [113]. Zhang et al. utilized desert sand ceramsite as an aggregate in the production of concrete, enabling the development of novel lightweight load-bearing wall materials with commendable energy-saving and thermal insulation properties [114]. Zhao et al. fabricated load-bearing prefabricated building block components by incorporating Dongguan Fansing Factory ceramsite as aggregate, achieving concrete with strength class LC35 and density class 1900 [115]. Zheng et al. employed a lightweight concrete mixture incorporating a reduced volume of shell structural ceramsite as an aggregate for non-load-bearing structures [116]. Bu et al. employed waste rubber ceramsite as aggregate in the production of lightweight wall panels, resulting in a significant reduction in the structural weight of buildings [117].

Finally, ceramsite lightweight concrete found applications in other fields as well. Lightweight high-strength ceramsite, with its excellent washout resistance and chemical stability, enabled the prepared concrete to maintain durability in harsh environments, making it suitable for infrastructure projects with high durability requirements. Furthermore, this type of concrete also demonstrated certain electromagnetic shielding capability and was consequently employed in applications requiring protection against electromagnetic interference. For example, Gao et al. investigated the use of ceramsite as aggregate to produce permeable concrete, which could be employed in sustainable and durable infrastructure projects [118]. The study conducted by Li et al. utilized ceramsite as an aggregate to fabricate permeable concrete, which exhibited potential applications in stormwater management and various infrastructure projects [119]. He et al. employed iron oxide ceramsite as an aggregate to fabricate wave-absorbent cementitious composites, which exhibit promising potential in safeguarding civil and military structures against electromagnetic interference, thereby offering a prospective application [120].

3.2. Mine roadway support

Lightweight high-strength ceramsite exhibited low density, excellent fire resistance and seismic performance, a low elastic modulus, and good corrosion resistance. Based on these properties, the lightweight concrete prepared with it as aggregate demonstrated good comprehensive physicomechanical characteristics, and its strength met the support requirements for underground roadways. This enabled it not only to fulfill the substantial demand for concrete materials in mine support but also to utilize industrial waste, aligning with the concept of green mining. Consequently, ceramsite lightweight high-strength concrete showed broad application prospects in mine underground support engineering. For example, Song et al. designed a ceramsite-rubber-fiber shotcrete with high thermal resistance and crack resistance using low thermal conductivity ceramsite as aggregate, addressing the significant shrinkage cracking of primary support shotcrete in high-geothermal mountain tunnels and deep hot mine roadways [121]. Chen et al. utilized ceramsite as an aggregate to prepare concrete. They reported that this concrete offered expedited and enhanced support for roadways, thereby providing scientific evidence and references for the application of ceramic concrete in coal mine shafts. The study conducted by Li et al. utilized fly ash ceramsite as an aggregate to formulate LC20 strength concrete, demonstrating its suitability for roadway support conditions in coal mines [122]. Wang utilized ceramsite as an aggregate in the preparation of lightweight high-strength concrete to fulfill the requirements for support strength, enabling its application in underground rocky roadway support with excellent effectiveness. Furthermore, this study provided scientific and effective technical parameters to promote the utilization of ceramic concrete in supporting rocky roadways [123]. Huang et al. utilized ceramsite as a lightweight aggregate to fabricate thermal insulation shotcrete, which demonstrated remarkable compatibility for withstanding high temperatures and providing reliable support for roadways in the surrounding rock of deep mines [124].

3.3. Marine engineering and construction

Marine engineering structures faced severe challenges during construction, including tidal impact and seawater corrosion (particularly chloride ion erosion). Lightweight high-strength ceramsite served as an ideal lightweight aggregate due to its high strength and excellent resistance to acid and alkali corrosion. The lightweight concrete prepared with it not only exhibited impact resistance, corrosion resistance, and good workability but also demonstrated exceptional resistance to chloride ion penetration. This effectively protected the internal steel reinforcement from corrosion, thereby significantly enhancing the structure's durability and service life in harsh marine environments, making it fully suitable for marine engineering construction.

In bridge construction, LWHSC incorporating ceramsite as a lightweight aggregate can be utilized for the paving layer of the bridge deck, as well as for the renovation and expansion of existing bridges. Notably, LWHSC has been employed in prominent projects such as the Chesapeake Bay Bridge in the United States (spanning 6500 m) and the Rhine River Bridge in Cologne, Germany (with a main span of 185 m). Additionally, LWHSC was successfully implemented in Norway's record-breaking pre-stressed concrete continuous rigid bridge span measuring 298 m [125]. Li et al. employed shale and clay ceramsite as the aggregate during the production of lightweight high-strength concrete, rendering it suitable for offshore structures to endure the challenging

circumstances of marine environments [126]. Research by Wang et al. indicated that concrete-filled FRP tube (CFFT) members utilizing seawater coral aggregate concrete (SCAC) instead of ordinary aggregate concrete (OAC) held great promise for marine engineering. The key mechanism was that the fiber-reinforced polymer (FRP) tube's resistance to chloride ion penetration addressed the fundamental issue of SCAC's poor corrosion resistance, making these composites an ideal alternative for piles and columns in corrosive marine settings [127]. Liu et al. developed concrete using coral aggregate, having average compressive and flexural strengths of 116.76 and 18.24 MPa, respectively. It was applicable for marine engineering and remote island construction [128].

3.4. Construction of highway foundations

In highway engineering, the pavement after completion needed to effectively block the transfer of surface temperature under both hot and cold conditions to prevent thermal disturbance-induced instability and damage to the underlying permafrost subgrade. Therefore, enhancing the thermal insulation performance of the pavement structure became a key technical issue in permafrost region highway construction. In this context, lightweight high-strength ceramsite concrete exhibited significant application advantages: its inherent low thermal conductivity provided the pavement with excellent insulation properties; at the same time, its good freeze-thaw resistance, impermeability, and resistance to water scour collectively ensured long-term durability and structural integrity of the pavement under harsh environmental conditions, making it highly suitable for construction in special areas such as permafrost regions. The study conducted by Yuan et al. highlighted that incorporating phase change materials and ceramsite as aggregates in pavement mixes exhibited excellent thermal resistance, effectively mitigating the rapid degradation of pavements under high-temperature conditions [129]. Chen developed a lightweight aggregate concrete by incorporating fly ash ceramsite as aggregates, demonstrating its remarkable ability to effectively reduce the heat transfer coefficient. This innovative approach not only achieves the desired goals of insulation and frost protection but also holds great potential for application in specialized highway construction [130]. Han et al. investigated the road performance of fly ash ceramsite concrete and found that it had lower thermal conductivity and permeability, higher freeze-thaw resistance, and sufficient wear resistance compared to ordinary concrete, demonstrating its application value in highway engineering [131].

4. Solidification strategies and clean production pathways for ceramsite

The presence of heavy metals in solid waste restricted their resource utilization. Currently, heavy metal treatment primarily relied on extraction and solidification/stabilization techniques. However, due to the complex composition and relatively low heavy metal content of most solid wastes, extraction methods often proved economically and technically inefficient. Consequently, solidification/stabilization became the preferred approach for such waste treatment. For sintered ceramsite, high-temperature pyrolysis served as a common technical method for solidification. When the temperature exceeded 1000 °C, the solidification effect of heavy metals became particularly significant. Most heavy metals could be stably fixed in the residue during pyrolysis. The high-temperature sintering process generated new phases including glass phase and pyroxene phase. The glass phase immobilized heavy metals through physical encapsulation within its network structure, while the pyroxene phase fixed heavy metal ions in the crystal lattice via isomorphous

substitution [49,132,133]. Additionally, some systems were capable of forming geopolymer structures, which achieved the stabilization of heavy metals through adsorption, encapsulation, and ion exchange (Figure 8). During the sintering process, the heavy metals in solid waste were transformed from more active forms (such as exchangeable and reducible forms) into more stable forms (such as oxidizable and residual forms), thereby significantly reducing their leaching concentration and leaching toxicity and enabling the final ceramsite products to meet safety standards. For NSC, cementitious materials like cement were primarily employed. The core mechanism involved hydration reactions that generated products such as calcium silicate hydrate (C-S-H) gel and ettringite, which immobilized heavy metal ions within the matrix through adsorption, encapsulation, chemical precipitation, and ion exchange (Figure 9). The evaluation of heavy metal leaching rates could be conducted with reference to the Identification Standards for Hazardous Waste-Identification of Leaching Toxicity and the Technical Specification for Co-processing Solid Wastes in Cement Kilns, with the leaching concentration limits for various heavy metals provided in Table 3.

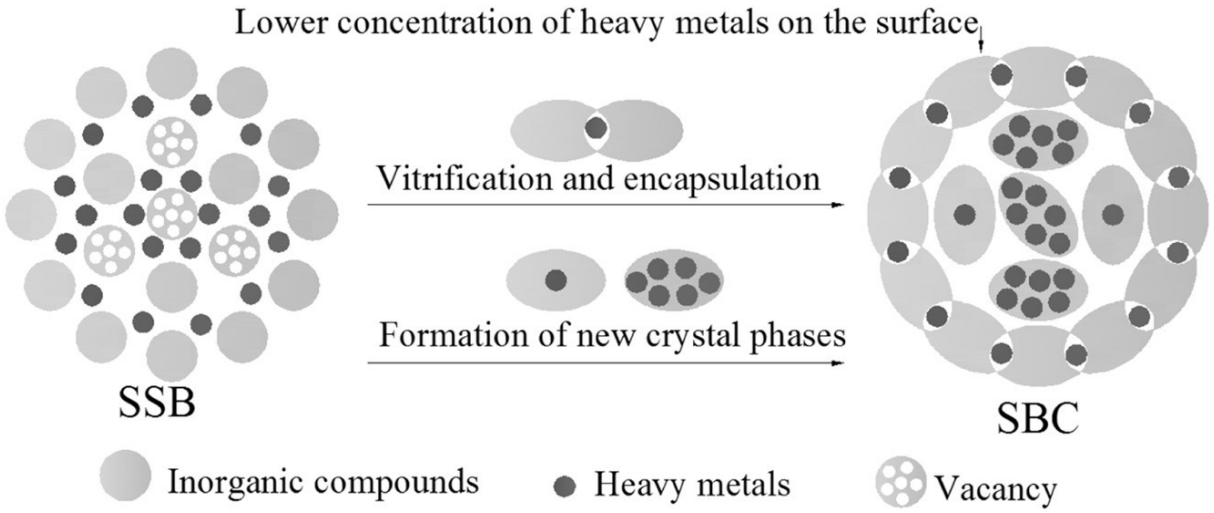

Figure 8. Heavy metals immobilization mechanisms in sludge biochar ceramsite (Reproduced from Ref. [136] with permission).

The aforementioned sintering-based solidification mechanism was well validated in practical applications. For instance, Pei et al. sintered ceramsite from red mud and waste wood chips at 1125 °C, and found that the leaching concentration of sodium ions-the primary harmful element in red mud-was only 12.3 mg/L, significantly lower than that of the original red mud (460 mg/L) [102]. Ke et al. demonstrated that using a raw material formulation of 65% MCS (metal-contaminated soil), 25% CG (coal gangue), 5% sodium metasilicate, and 5% borax to produce ceramsite, followed by sintering at 1000 °C, achieved immobilization rates exceeding 90% for Cu, Mn, Ni, and Zn. The resulting products complied with the GB/T 30760-2024 standard for leaching toxicity [73]. Liu et al. produced ceramsite from desert sand and fly ash sintered at 1125 °C, and found that the solidification rates of Cr, Ba, Zn, Cu, etc., exceeded 98%, demonstrating excellent stability and solidification capacity for heavy metals [134]. Xu synthesized NSC using fly ash, GGBFS (ground granulated blast furnace slag), and FGDG (flue gas desulfurization gypsum) with cement as an additive. This resulted in a reduction of the leaching rate of Cr from 2.54% to 0.15%. The Cr was originally present in high

content in DFA (dechlorinated municipal solid waste incineration fly ash) and its leaching concentration from 0.5388 to 0.0088 mg/L, representing decreases by approximately 16-fold and 60-fold, respectively [135]. Han et al. prepared NSC using a 100% raw material system comprising PT (phosphate tailing), FA (fly ash), SR (soda residue), and GGBS (granulated blast furnace slag). The release concentrations of Cd, Pb, Cr, Ni, As, and Cu were all far below the permissible regulatory limits [46]. Ceramsite produced via mature processes exhibited effectively controlled heavy metal leaching concentrations within the national standard limits, demonstrating that its application as lightweight aggregate in engineering projects provided reliable assurance of environmental safety.

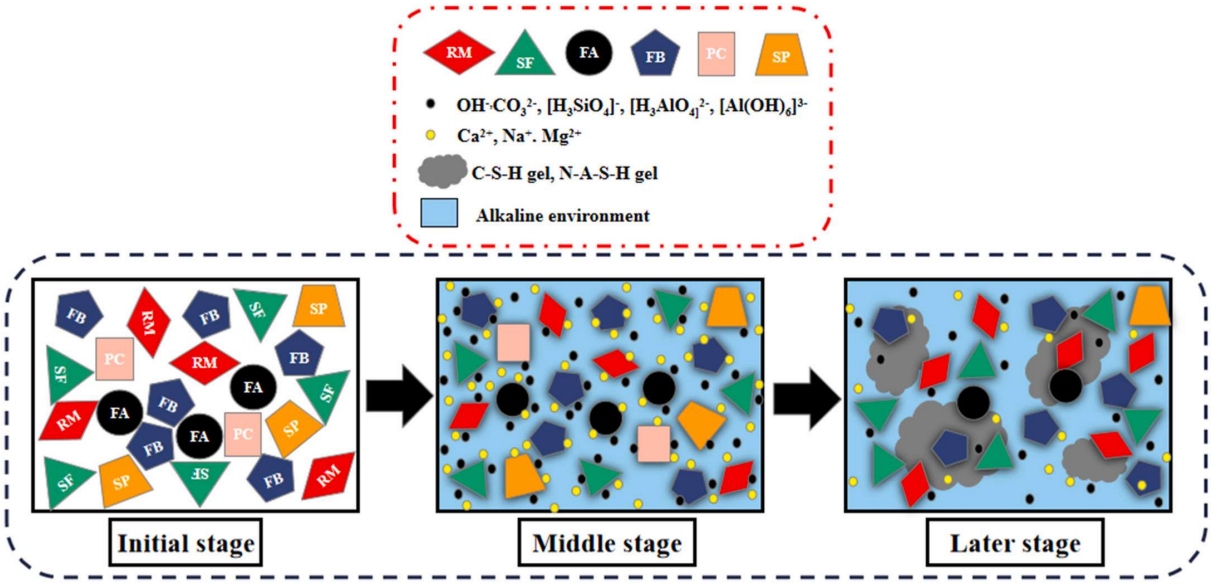

Figure 9. The coupling mechanism of heavy metals in unburned ceramsite (Reproduced from Ref. [137] with permission).

Table 3. Standard for heavy metal leaching from solid waste ceramics.

Ceramsite standard	Item (mg·L^{-1})	Heavy metal									Ref.
		Cd	Cr (VI)	As	Hg	Cu	Zn	Pb	Ba	Ni	[143]
	Control limit	≤1	≤15	≤5	≤0.1	≤100	≤100	≤5	≤100	≤5	

During the sintering process of solid waste ceramsite, a comprehensive multi-level control system was established for pollutants such as dioxins (emission limit: 0.1 ng TEQ/m^3), volatile heavy metals, NO_x (emission limit: 300 mg/m^3), and Cl (emission limit: 60 mg/m^3) present in raw materials including municipal solid waste incineration bottom ash and sludge. Dioxins were efficiently decomposed and their formation was suppressed through the synergistic effect of high-temperature retention (≥850 °C) and a high sulfur-to-chlorine ratio (S/Cl ≈ 20) in the raw materials (Figure 10). Heavy metals were stabilized and solidified within the ceramsite matrix during high-temperature sintering, with volatile components being further treated by flue gas purification technologies such as activated carbon adsorption. The NO_x emission concentration (approximately 471.6 mg/m^3) was inherently lower than the national standard, and mature deep treatment technologies were available to ensure further reduction. MSWI fly ash, which contained chloride salts, underwent hydrothermal

desalination pretreatment to remove a significant amount of soluble chlorides, thereby preventing it from providing a chlorine source that could drive low-temperature dioxin synthesis during sintering and cooling. By combining raw material pretreatment (e.g., microwave decomposition, chemical stabilization) with end-of-pipe treatment processes, the final emission concentrations of all pollutants were well below the strictest EU and national limits, demonstrating that pollutant emission risks from the solid waste ceramsite sintering process were comprehensively and effectively controlled under standard operating conditions [138–140]. Qiu et al. demonstrated that after microwave treatment at 220 °C for 2 h with 10 wt% Na_2HPO_4 as an additive, the degradation efficiency of PCDD/Fs in MSWI fly ash (initial total concentration: 180882 pg g^{-1}) reached 91.8%, and its toxicity equivalent (WHO-TEQ) was correspondingly reduced to 0.255 ng kg^{-1} [141]. Additionally, Yang et al. confirmed that the high chloride salt content (32.28% of the MSWI fly ash) was a key factor driving dioxin synthesis. Through a pre-washing process, 83.05% of the soluble chlorides were effectively removed, reducing the chloride salt content significantly to 5.47%, thereby suppressing dioxin formation at the source [142].

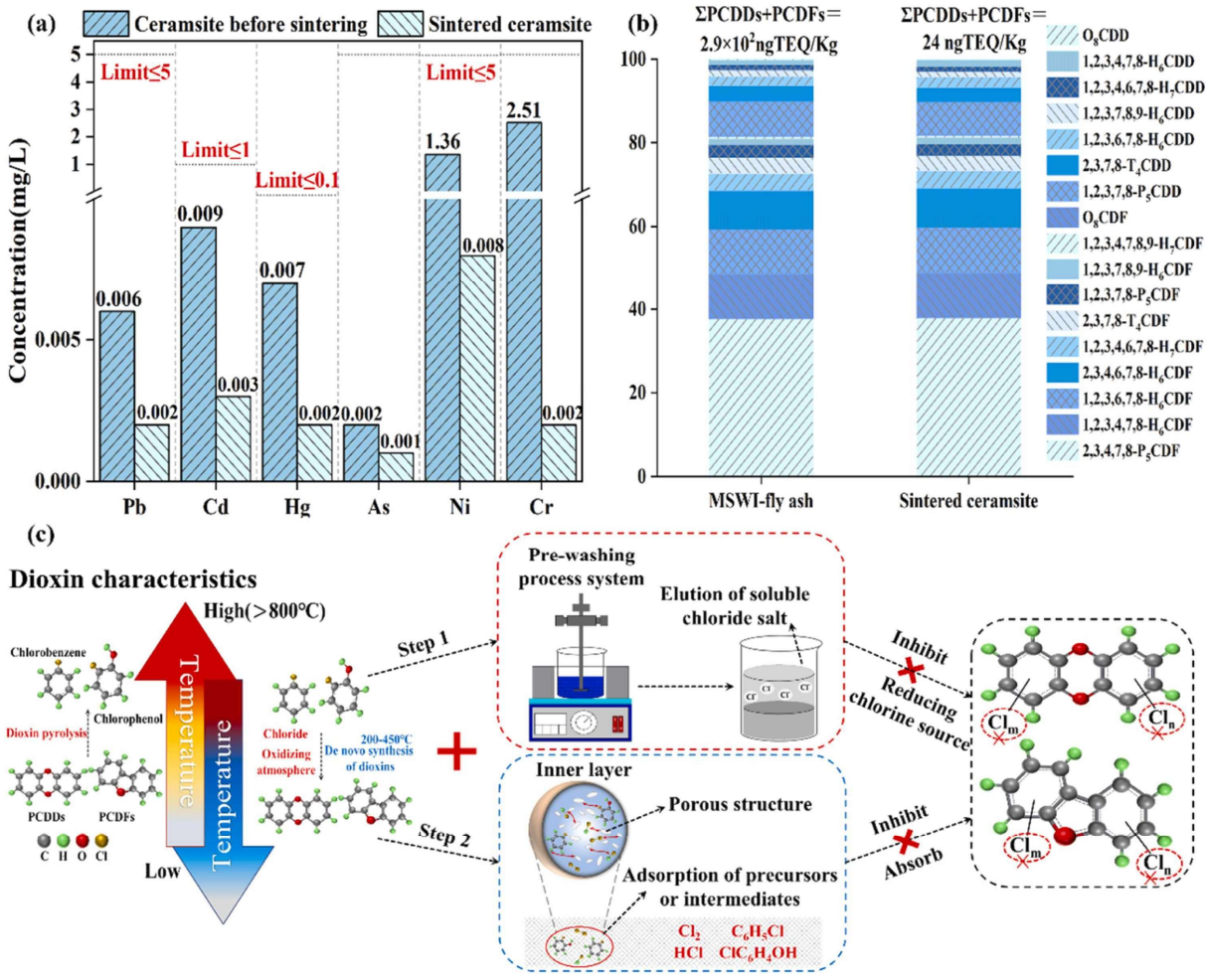

Figure 10. (a) the leaching concentration of heavy metals in ceramsite before and after sintering; (b) the total amount and types of dioxins in MSWI fly ash and sintered ceramsite; (c) dioxin inhibition mechanism of process system (Reproduced from Ref. [142] with permission).

5. Conclusions and outlook

This review systematically analyzes the preparation, performance regulation mechanisms, applications, and environmental benefits of solid waste-based ceramsite, leading to the following key conclusions:

(1) Solid wastes exhibit great potential as functional components: in addition to serving as raw materials for ceramsite production, they can act as highly efficient pore-forming agents. Through synergistic preparation strategies, this approach facilitates the development of lightweight ceramsite while converting wastes into value-added products, thereby achieving dual objectives of environmental management and resource valorization.

(2) The environmental advantages of solid waste-based ceramsite are manifested throughout its life cycle: it enables large-scale consumption of various solid wastes at the source; effectively immobilizes heavy metals and other hazardous substances during processing via high-temperature sintering or chemical bonding; and demonstrates significant reduction potential in energy consumption and carbon footprint in the final product compared to natural aggregates, particularly through the utilization of inherent energy in solid wastes and process optimization.

(3) Sintered and non-sintered ceramsite technologies exhibit complementary characteristics: sintered ceramsite offers the advantage of simultaneously achieving high strength and low water absorption through the formation of liquid and crystalline phases at high temperatures, with broad performance tunability and mature technology. In contrast, NSC is characterized by low energy consumption, low carbon emissions, and simple processing. However, its strength development typically relies on the formation of cementitious products, resulting in gaps in absolute strength and durability compared to high-performance sintered ceramsite.

(4) The macroscopic properties of ceramsite (density, strength, water absorption) are not independent parameters but are collectively governed by its internal multiscale structural characteristics, including phase composition (e.g., glass phase, mullite), pore structure (amount, morphology, distribution), and interfacial bonding state. Understanding this structure-performance relationship is fundamental to the precise regulation of ceramsite performance.

Based on current research consensus and gaps, the following future research directions are proposed:

(1) Current studies predominantly focus on enhancing individual properties of ceramsite (e.g., strength or density). Future work should strengthen research on the intrinsic mechanisms governing the interdependent relationships among key properties such as density, strength, and water absorption, enabling synergistic performance regulation through multi-objective optimization.

(2) There is a lack of systematic data on the long-term durability and in-service performance of solid waste-based ceramsite concrete under realistic conditions, such as complex stress states, wet-dry cycles, and freeze-thaw erosion. There is an urgent need to conduct long-term monitoring and accelerated testing to establish predictive service life models, providing reliable design basis for engineering applications.

(3) Efforts should be directed toward developing novel, highly efficient low-temperature activators and optimizing curing regimes to significantly improve the early-age strength, ultimate strength, and dimensional stability of NSC, thereby narrowing its performance gap with sintered ceramsite and consolidating its low-carbon advantages.

Use of AI tools declaration

The authors declare they have not used Artificial Intelligence (AI) tools in the creation of this article.

Acknowledgement

This study was financially supported by the Key Research and Development Program of Wuhan (2023020402010624) and National Natural Science Foundation of China (52304191).

Author contributions

Haipeng Liu: writing–review & editing, validation; Nanyan Hu: writing–original draft, data curation; Qigao Li: methodology, resources; Shengwen Yang: methodology, investigation; Yicheng Ye: funding acquisition, project administration, writing–review & editing; Jie Wang: methodology, resources; Hongping Wang: methodology, resources.

Conflict of interest

The authors declare no conflict of interest.

References

1. Tian C, Zhao L, He XY, et al. (2024) Enhancing mechanism of mechanical properties of lightweight and high-strength concrete prepared with autoclaved silicate lightweight aggregate. *J Build Eng* 98: 111102. https://doi.org/10.1016/j.jobe.2024.111102
2. Zou S, Lu JX, Xiao J, et al. (2023) Development and characteristics of novel high-strength lightweight core-shell aggregate. *Constr Build Mater* 393: 132080. https://doi.org/10.1016/j.conbuildmat.2023.132080
3. Gu DG, Oh JH, Yoo SW (2023) Evaluation of bond-slip behavior of high strength lightweight concrete with compressive strength 120 MPa and unit weight 20 kN/m^3. *J Korean Recycl Constr Res Inst* 11: 39–47. https://doi.org/10.14190/JRCR.2023.11.1.39
4. Li M, Wang Y, Ren J, et al. (2024) Evaluation and prediction of fatigue life for ceramsite lightweight concrete considering the effects of ceramsite aggregate size and content. *Case Stud Constr Mater* 21: e03613. https://doi.org/10.1016/j.cscm.2024.e03613
5. Eisa AS, Aboul-Nour LA, Mohamad A (2024) Experimental and theoretical investigation on the bond strength between high-strength and lightweight concrete. *Matéria (Rio J)* 29: e20230312. https://doi.org/10.1590/1517-7076-rmat-2023-0312
6. Patiño-Mora K, María HS, Jünemann R (2025) Experimental assessment of reinforced concrete squat walls with high-strength lightweight concrete. *Mater Struct* 58: 237. https://doi.org/10.1617/s11527-025-02756-0
7. Shang M, Qiao H, He Z, et al. (2023) Study on the shrinkage mechanism and prediction model of high-strength specified density concrete based on the internal curing micro-pump effect of MSW incineration tailings. *Constr Build Mater* 372: 130804. https://doi.org/10.1016/j.conbuildmat.2023.130804

8. Liu H, Elchalakani M, Karrech A, et al. (2021) High strength flowable lightweight concrete incorporating low C_3A cement, silica fume, stalite and macro-polyfelin polymer fibres. *Constr Build Mater* 281: 122410. https://doi.org/10.1016/j.conbuildmat.2021.122410
9. Gao Y, Han X, Su X (2025) Research on the design method of elastic modulus of ceramsite lightweight aggregate concrete. *Constr Build Mater* 495: 143593. https://doi.org/10.1016/j.conbuildmat.2025.143593
10. Wang Y, Zhang W, Wang J, et al. (2024) Effects of coarse aggregate size on thickness and micro-properties of ITZ and the mechanical properties of concrete. *Cem Concr Compos* 154: 105777. https://doi.org/10.1016/j.cemconcomp.2024.105777
11. Sun W, Wu Y, Yuan J, et al. (2025) Experimental and simulation studies on the anti-penetration performance of high-strength concrete incorporated with new green ceramsite aggregate. *Constr Build Mater* 489: 142173. https://doi.org/10.1016/j.conbuildmat.2025.142173
12. Bekkeri GB, Shetty KK, Nayak G (2024) Performance of concrete produced with alkali-activated artificial aggregates. *J Mater Cycles Waste* 26: 2024–2042. https://doi.org/10.1007/s10163-024-01938-2
13. Zhou Y, Geng O, Zhao Y, et al. (2024) Enhancement mechanism of compressive plastic deformation properties in concrete induced by fiber spherical aggregates. *Constr Build Mater* 441: 137564. https://doi.org/10.1016/j.conbuildmat.2024.137564
14. Jiang H, Wu LJ, Guan L, et al. (2024) Durability life evaluation of marine infrastructures built by using carbonated recycled coarse aggregate concrete due to the chloride corrosive environment. *Front Mar Sci* 11: 1357186. https://doi.org/10.3389/fmars.2024.1357186
15. Ying H, Wang S, Lu Z, et al. (2023) Development and thermal response of concrete incorporated with multi-stage phase change materials-aggregates for application in seasonally frozen regions. *J Build Eng* 71: 106562. https://doi.org/10.1016/j.jobe.2023.106562
16. Liu S, Yang CR, Liu W, et al. (2020) A novel approach to preparing ultra-lightweight ceramsite with a large amount of fly ash. *Front Environ Sci Eng* 14: 62. https://doi.org/10.1007/s11783-020-1241-1
17. Zhang PQ, Shen DS, Shao JY, et al. (2024) Green synthesis of Fe_3O_4@ceramsite from sludge improving anaerobic digestion performance of waste activated sludge. *J Environ Manage* 359: 121085. https://doi.org/10.1016/j.jenvman.2024.121085
18. Shi XF, Geng C, Li QM, et al. (2024) A novel application for magnetite tailings and municipal sludge in ceramsite preparation. *Environ Prog Sustain* 43: e14239. https://doi.org/10.1002/ep.14239
19. Zhong MY, Meng J, Ning BK, et al. (2024) Preparation and alkali excitation mechanism of coal gangue-iron ore tailings non-sintering ceramsite. *Constr Build Mater* 426: 136209. https://doi.org/10.1016/j.conbuildmat.2024.136209
20. Jiang J, Wang Y, Li JW, et al. (2024) Characterization and mechanism of sintered light aggregate ceramsite with engineering excavated soil. *Structures* 70: 107699. https://doi.org/10.1016/j.istruc.2024.107699
21. Li X, Wang P, Guo Z, et al. (2022) Effect of Fe^{2+}/Fe^{3+} on high-strength ceramsite prepared by sintering geopolymers using iron ore tailings. *Ceram Int* 48: 5681–5688. https://doi.org/10.1016/j.ceramint.2021.11.113

22. Ma W, Pan J, Zhu D, et al. (2025) Properties optimization of high-strength ceramsite prepared from coal gangue and iron ore tailings. *Constr Build Mater* 493: 143294. https://doi.org/10.1016/j.conbuildmat.2025.143294
23. Jiang J, Chen S, Jin C, et al. (2023) Preparation and properties of high-strength lightweight aggregate ceramsite from nepheline tailings. *Constr Build Mater* 368: 130458. https://doi.org/10.1016/j.conbuildmat.2023.130458
24. Zhao SK, Wu JJ, Xu JQ, et al. (2025) Structure and properties of high-strength lightweight ceramsite prepared by synergistic sintering of iron tailings, inorganic sludge, and recycled micro-powder. *Mater Today Commun* 48: 113598. https://doi.org/10.1016/j.mtcomm.2025.113598
25. Chai YF, Hu WX, Zhang YH, et al. (2023) Process and property optimization of ceramsite preparation by Bayan Obo tailings and blast furnace slag. *J Iron Steel Res Int* 30: 1381–1389. https://doi.org/10.1007/s42243-023-00991-9
26. Zhao H, Wang XY, Zhang XS, et al. (2024) Preparation of high-strength ceramsite via co-sintering of shield tunnel muck and steel slag: Correlation investigation on phase composition and particle strength. *Constr Build Mater* 439: 137413. https://doi.org/10.1016/j.conbuildmat.2024.137413
27. Peng C, Dai GF, Wang YH, et al. (2024) Preparation of high-strength ceramsite from coal gangue and printing and dyeing sludge: Design strategy and modelling mechanism. *Ceram Int* 50: 19963–19970. https://doi.org/10.1016/j.ceramint.2024.03.122
28. General Administration of Quality Supervision, Inspection and Quarantine of the People's Republic of China (2010) Lightweight aggregates and test methods—Part 1: Lightweight aggregates: GB/T 17431.1-2010. Beijing: Standards Press of China.
29. Zhang C, Ren Z, Wang L, et al. (2024) The synergistic sintering of ultra-lightweight ceramsite from molybdenum ore tailings, iron ore tailings and waste glass powders: Properties and formation mechanism. *Constr Build Mater* 452: 138852. https://doi.org/10.1016/j.conbuildmat.2024.138852
30. Zeng H, Li X, Sun W, et al. (2024) Co-utilization of stone coal leaching slag and bauxite residue for the preparation of lightweight ceramsite. *Constr Build Mater* 431: 136541. https://doi.org/10.1016/j.conbuildmat.2024.136541
31. Kang JY, Song XY, Chen JF (2025) Experimental study on the preparation of lightweight ceramsite using engineering excavated soil. *New Build Mater* 52: 89–94. https://doi.org/10.3969/j.issn.1001-702X.2025.02.020
32. Fei YH, Li XL, Shao GB, et al. (2024) Experimental study on the preparation of ceramsite by co-combustion of oily sludge with slag and fly ash. *Environ Pollut Control* 46: 1628–1632. https://doi.org/10.15985/j.cnki.1001-3865.202312048
33. Riley CM (1951) Relation of chemical properties to the bloating of clays. *J Am Ceram Soc* 34: 59–136. https://doi.org/10.1111/j.1151-2916.1951.tb11619.x
34. Wang H, Zhang Q, Bian J, et al. (2023) Synergistic coagulation effect of the cationic coagulant and anionic flocculant on fluorite tailings. *Environ Technol Innovation* 30: 103096. https://doi.org/10.1016/j.eti.2023.103096
35. Ruan M, Tian Q, Zhang M, et al. (2024) Fabrication and characterization of foam ceramics from recycled waste concrete powder and waste glass powder. *Constr Build Mater* 451: 138807. https://doi.org/10.1016/j.conbuildmat.2024.138807

36. Long Y, Pu K, Yang Y, et al. (2023) Preparation of high-strength ceramsite from municipal solid waste incineration fly ash and clay based on CaO-SiO_2-Al_2O_3 system. *Constr Build Mater* 368: 130492. https://doi.org/10.1016/j.conbuildmat.2023.130492
37. Liu Z, Guo R, Pan T, et al. (2023) Preparation of ceramsite from low-silicon red mud (LSRM): Effects of Si–Al ratio and sintering temperature. *Ceram Int* 49: 34191–34204. https://doi.org/10.1016/j.ceramint.2023.08.131
38. Wang Y, Xiao TT, Hu XL, et al. (2025) Preparation of lightweight ceramsite from weathered granite washing sludge: Reinforcing roles of MgO and Na_2O and thermal analysis. *Chem Eng J* 521: 166694. https://doi.org/10.1016/j.cej.2025.166694
39. Wang XX, Qin YH, Okeke I, et al. (2024) Revealing the intrinsic sintering mechanism of high-strength ceramsite from CFB fly ash: Focus on the role of CaO. *Ceram Int* 50: 24281–24292. https://doi.org/10.1016/j.ceramint.2024.04.158
40. Wang CW, Wang YX, Sun W, et al. (2022) Thermodynamic assessment of iron and the expansion behavior of porous ceramsite in pure mineral systems relating to solid waste components. *Ceram Int* 48: 32867–32876. https://doi.org/10.1016/j.ceramint.2022.07.214
41. Wang YX, Yang AQ, Wang F, et al. (2025) Thermodynamics-driven valorization of fluorite tailings into sustainable lightweight ceramsite: Phase evolution, sintering mechanisms, and circular economy potential. *J Environ Chem Eng* 13: 117950. https://doi.org/10.1016/j.jece.2025.117950
42. Huang Y, Hu NY, Ye YC, et al. (2022) Preparation and pore-forming mechanism of MgO-Al_2O_3-CaO-based porous ceramics using phosphorus tailings. *Ceram Int* 48: 29882–29891. https://doi.org/10.1016/j.ceramint.2022.06.253
43. Liu Z, Guo RX, Wang XY, et al. (2023) Construction ceramsite from low-silicon red mud: Design, preparation, and sintering mechanism analysis. *Process Saf Environ* 176: 166–179. https://doi.org/10.1016/j.psep.2023.06.017
44. Shen F, Wei GS, Qiao LG, et al. (2022) Sintering process optimization of phosphorous tailings ceramsite and preparation of lightweight ultra-high strength concrete. *J Guilin Univ Technol* 42: 717–724. https://doi.org/10.3969/j.issn.1674-9057.2022.03.025
45. Li XY (2016) Experimental study on sintering process and resource utilization of phosphorous tailings ceramsite. Master theses, Chongqing University.
46. Han R, Leng H, Luo H, et al. (2025) Turning waste into treasure: Preparation, physical properties and microstructure of alkali-activated phosphorus tailings-based fully solid waste non-sintered lightweight aggregates. *J Clean Prod* 527: 146693. https://doi.org/10.1016/j.jclepro.2025.146693
47. Lv YF, Hu NY, Ye YC, et al. (2023) Adsorption of Ag^+ with NaCl modified ceramsite prepared from total phosphorus tailings: Performance and adsorption mechanism. *Water Air Soil Poll* 234: 784. https://doi.org/10.1007/s11270-023-06797-5
48. Sun YH, Li JS, Chen Z, et al. (2021) Production of lightweight aggregate ceramsite from red mud and municipal solid waste incineration bottom ash: Mechanism and optimization. *Constr Build Mater* 287: 122993. https://doi.org/10.1016/j.conbuildmat.2021.122993
49. Shao YY, Tian C, Kong WJ, et al. (2023) Co-utilization of zinc contaminated soil and red mud for high-strength ceramsite: Preparation, zinc immobilization mechanism and environmental safety risks. *Process Saf Environ* 170: 491–497. https://doi.org/10.1016/j.psep.2022.12.038

50. Shi YX, Guo WC, Jia YL, et al. (2022) Preparation of non-sintered lightweight aggregate ceramsite based on red mud-carbide slag-fly ash: Strength and curing method optimization. *J Clean Prod* 372: 133788. https://doi.org/10.1016/j.jclepro.2022.133788
51. Wan Q, Han QJ, Zhang XY, et al. (2019) Preparation and performance optimization of novel ceramsite from waterworks sludge. *Bull Chin Ceram Soc* 38: 1228–1236. https://doi.org/10.16552/j.cnki.issn1001-1625.2019.04.049
52. Sun WH, Xia CK, Yao JG, et al. (2019) Experimental study on preparation of high-strength ceramsite from quarry tailings mud and municipal sludge. *Non-Metall Mines* 42: 25–28. https://doi.org/10.3969/j.issn.1000-8098.2019.01.008
53. Peng Z, Shen D, Wang X, et al. (2025) Facile route for preparing high-strength ceramsite from sewage sludge and clay. *Constr Build Mater* 484: 141812. https://doi.org/10.1016/j.conbuildmat.2025.141812
54. Yang XW (2021) Preparation of high-strength ceramsite based on hazardous waste and research on heavy metal stabilization/solidification mechanism. Master theses, Qilu University of Technology.
55. Wu XT, Gu FQ, Su C, et al. (2022) Preparing high-strength ceramsite from ferronickel slag and municipal solid waste incineration fly ash. *Ceram Int* 48: 34265–34272. https://doi.org/10.1016/j.ceramint.2022.07.357
56. Zhu Y, Shao YY, Tian C, et al. (2024) Preparation of municipal solid waste incineration fly ash/granite sawing mud ceramsite and the morphological transformation and migration properties of chlorine. *Waste Manage* 173: 1–9. https://doi.org/10.1016/j.wasman.2023.10.039
57. Wang PQ (2020) Polycondensation and sintering mechanism of lightweight ceramsite and its application in concrete. Master theses, Chang'an University.
58. Wang L, Tian HX, Lei WY, et al. (2024) Development of high-strength ceramsite via sintering of iron ore tailings: Process optimization and properties. *Constr Build Mater* 457: 139440. https://doi.org/10.1016/j.conbuildmat.2024.139440
59. Ma WZ, Zhang WJ, Pan J, et al. (2025) Synergistic mechanism for preparation of high-performance ceramsite from coal gangue and iron ore tailings. *Process Saf Environ* 201: 107591. https://doi.org/10.1016/j.psep.2025.107591
60. Wang LS, Wang YX, Sun W, et al. (2023) Preparation of lightweight and high-strength ceramsite from highly doped coal fly ash. *Trans Nonferrous Met Soc China* 33: 3885–3898. https://doi.org/10.1016/s1003-6326(23)66378-2
61. Qin J, Cui C, Cui XY, et al. (2015) Preparation and characterization of ceramsite from lime mud and coal fly ash. *Constr Build Mater* 95: 10–17. https://doi.org/10.1016/j.conbuildmat.2015.07.106
62. Jia GH, Wang YL, Yang FL, et al. (2023) Preparation of CFB fly ash/sewage sludge ceramsite and the morphological transformation and release properties of sulfur. *Constr Build Mater* 373: 130864. https://doi.org/10.1016/j.conbuildmat.2023.130864
63. Li Y, Zhao W, Zhang XH, et al. (2023) Preparation and performance study of high-strength fluorite tailings ceramsite. *Inorg Chem Ind* 55: 100–108. https://doi.org/10.19964/j.issn.1006-4990.2022-0397
64. Liu GF, Zeng CC, Wang ZK, et al. (2023) Preparation and performance study of high-strength sintered ceramsite from tungsten smelting slag. *Inorg Chem Ind* 55: 132–139. https://doi.org/10.19964/j.issn.1006-4990.2022-0624

65. Ma C, Bao S, Zhang Y, et al. (2022) Preparation of non-sintered sewage sludge based ceramsite by alkali-thermal activation and hydration mechanism. *Ceram Int* 48: 31606–31613. https://doi.org/10.1016/j.ceramint.2022.07.082
66. Pan X, Liu J, Qi Y, et al. (2025) Preparation and formation mechanism of ultra-lightweight ceramsite from high-calcium red mud. *Constr Build Mater* 490: 142484. https://doi.org/10.1016/j.conbuildmat.2025.142484
67. Chen R, Pan Z, Chu S, et al. (2022) Optimize the preparation of novel pyrite tailings based non-sintered ceramsite by plackett-burman design combined with response surface method for phosphorus removal. *Front Chem* 10: 850171. https://doi.org/10.3389/fchem.2022.850171
68. Wang H, Zhang X, Huang X, et al. (2025) Insight into the microstructural evolution and fluorine migration mechanism of lightweight ceramsite derived from fluorite tailings. *J Environ Chem Eng* 13: 118140. https://doi.org/10.1016/j.jece.2025.118140
69. Sun X, Niu S, Cheng S, et al. (2025) Preparation of sintered ceramsite by synergising different types of expansion agents with multiple bulk solid wastes. *Constr Build Mater* 484: 141873. https://doi.org/10.1016/j.conbuildmat.2025.141873
70. Xiao T, Fan X, Zhou C, et al. (2024) Preparation of ultra-lightweight ceramsite from waste materials: Using phosphate tailings as pore-forming agent. *Ceram Int* 50: 15218–15229. https://doi.org/10.1016/j.ceramint.2024.01.441
71. Xu F, Liu W, Bu S, et al. (2022) Manufacturing non-sintered ceramsite from incinerated municipal solid waste ash (IMSWA): Production and performance. *Process Saf Environ* 163: 116–130. https://doi.org/10.1016/j.psep.2022.05.007
72. Zheng D, Li Z, Pang Q, et al. (2025) Preparation strategy and performance development mechanism of river sediment based non-sintered lightweight aggregate. *Constr Build Mater* 473: 141061. https://doi.org/10.1016/j.conbuildmat.2025.141061
73. Ke GP, Zeng W, Liu JY, et al. (2025) Metal transformation, immobilization, and risks in ceramsite production via co-sintering of metal-contaminated soil and coal gangue. *Fuel* 401: 135830. https://doi.org/10.1016/j.fuel.2025.135830
74. Li X, Geng J, Niu S, et al. (2025) Co-synthesis of lightweight aggregates from coal-biomass co-combustion ash and red mud: Optimization, properties, and environmental assessment. *Constr Build Mater* 492: 143097. https://doi.org/10.1016/j.conbuildmat.2025.143097
75. Song XC, Du S, Deng CN, et al. (2026) What are the carbon reduction benefits of regenerating ceramsite from solid waste? A new perspective on carbon footprint. *Environ Impact Assess Rev* 116: 108077. https://doi.org/10.1016/j.eiar.2025.108077
76. Li X, Geng J, Niu SL (2025) Ultra-lightweight ceramsite prepared from coal-biomass co-combustion ash and retired photovoltaic glass: Microstructure and sintering characteristics. *Ceram Int* 51: 53246–53258. https://doi.org/10.1016/j.ceramint.2025.09.075
77. Gao W, Zhang H, Ren Q, et al. (2023) A low-carbon approach to recycling engineering muck to produce non-sintering lightweight aggregates: Physical properties, microstructure, reaction mechanism, and life cycle assessment. *J Clean Prod* 385: 135650. https://doi.org/10.1016/j.jclepro.2022.135650
78. Li X, He C, Lv Y, et al. (2021) Effect of sintering temperature and dwelling time on the characteristics of lightweight aggregate produced from sewage sludge and waste glass powder. *Ceram Int* 47: 33435–33443. https://doi.org/10.1016/j.ceramint.2021.08.250

79. Wang Y, Liu X, Tang B, et al. (2021) Effect of Ca/(Si + Al) on red mud based eco-friendly revetment block: Microstructure, durability and environmental performance. *Constr Build Mater* 304: 124618. https://doi.org/10.1016/j.conbuildmat.2021.124618
80. Mi H, Yi L, Wu Q, et al. (2021) Preparation of high-strength ceramsite from red mud, fly ash, and bentonite. *Ceram Int* 47: 18218–18229. https://doi.org/10.1016/j.ceramint.2021.03.141
81. Zhang W, Zhao Q, Peng S, et al. (2025) Preparation and property evolution mechanism of high sludge-content ceramsite with blast furnace slag and red mud. *Water Process Eng* 71: 107284. https://doi.org/10.1016/j.jwpe.2025.107284
82. Liu J, Gao Y, Wang Y, et al. (2024) Non-sintered ceramsite from alkali-activated gasification slag for adsorption through the regulation of physical properties and pore structure. *J Clean Prod* 477: 143820. https://doi.org/10.1016/j.jclepro.2024.143820
83. Zhang LX, Liang LS, Li Y, et al. (2024) Preparation of lightweight foam glass-ceramics from copper slag tailings: Secondary aluminum slag as pore-forming agent. *Ceram Int* 50: 43699–43709. https://doi.org/10.1016/j.ceramint.2024.08.221
84. Chen S, Zhou J, Bie Y, et al. (2024) Sustainable ecological non-sintered ceramsite (senc) with alkali activators: Performance regulation and microstructure. *Sustainability* 16: 6634. https://doi.org/10.3390/su16156634
85. Xu N, Ma S, Wang N, et al. (2024) Optimization of ternary activator for enhancing mechanical properties of carbonized cementitious material based on circulating fluidized bed fly ash. *Processes* 12: 289. https://doi.org/10.3390/pr12020289
86. Mañosa J, Formosa J, Giro-Paloma J, et al. (2021) Valorisation of water treatment sludge for lightweight aggregate production. *Constr Build Mater* 269: 121335. https://doi.org/10.1016/j.conbuildmat.2020.121335
87. Xiao TT, Wang Y, Fan XY, et al. (2024) Preparation of eco-friendly and high-strength ceramsite by granite scraps, granite fine mud, and phosphogypsum: Response surface methodology optimization, environmental safety assessment. *Process Saf Environ* 192: 960–972. https://doi.org/10.1016/j.psep.2024.10.085
88. Luo YQ, Wang Y, Ma YQ, et al. (2025) Optimized preparation of dredged sediment-based functional ceramsite: thermodynamic profiling and formation mechanism. *Environ Res* 286: 122973. https://doi.org/10.1016/j.envres.2025.122973
89. Li CB, Zhang GF, Liu DZ, et al. (2023) Preparation of lightweight ceramsite from solid waste lithium slag and fly ash. *Constr Build Mater* 398: 132419. https://doi.org/10.1016/j.conbuildmat.2023.132419
90. Huang W, Gong MZ, Huang QW, et al. (2025) Research progress on the industrial solid waste-based ceramsite: Composition, curing and application. *Mater Today Commun* 49: 113769. https://doi.org/10.1016/j.mtcomm.2025.113769
91. Ding ZD, Sun JY (2022) Effect of compounding ground slag with perlite tailings on the properties of non-sintered ceramsite. *Bull Chin Ceram Soc* 41: 513–519. https://doi.org/10.16552/j.cnki.issn1001-1625.2022.02.024
92. Shahane HA, Patel S (2021) Influence of curing method on characteristics of environment-friendly angular shaped cold bonded fly ash aggregates. *J Build Eng* 35: 101997. https://doi.org/10.1016/j.jobe.2020.101997

93. Cao Y, Liu R, Han Y, et al. (2020) Nonsintered lightweight aggregates produced from waste sludge and its characteristics affected by additives. *Environ Prog Sustain* 39: e13389. https://doi.org/10.1002/ep.13389
94. Zhang X, Zhu F, Zhang Y, et al. (2024) Comprehensive utilization of red mud and blast furnace dust: Synergistic preparation of direct reduced iron and functional ceramsite. *Sep Purif Technol* 345: 127436. https://doi.org/10.1016/j.seppur.2024.127436
95. Ma J, Shi Y, Zhang H, et al. (2021) Crystallization of CaO–MgO–Al_2O_3–SiO_2 glass ceramic derived from blast furnace slag via one-step method. *Mater Chem Phys* 261: 124213. https://doi.org/10.1016/j.matchemphys.2020.124213
96. Yu L, Zhang Y, Mao H, et al. (2023) Structure evolution, properties and synthesis mechanism of ultra-lightweight eco-friendly ceramics prepared from kaolin clay and sewage sludge. *J Environ Chem Eng* 11: 109061. https://doi.org/10.1016/j.jece.2022.109061
97. Li XL, Zeng H, Sun N, et al. (2023) Preparation of lightweight ceramsite by stone coal leaching slag, feldspar, and pore-forming reagents. *Constr Build Mater* 370: 130642. https://doi.org/10.1016/j.conbuildmat.2023.130642
98. Nguyen HP, Mueller A, Nguyen VT, et al. (2021) Development and characterization of lightweight aggregate recycled from construction and demolition waste mixed with other industrial by-products. *Constr Build Mater* 313: 125472. https://doi.org/10.1016/j.conbuildmat.2021.125472
99. Cheng Y, Li J, Qin C, et al. (2023) Template-free route to fabricate extra-lightweight ceramsite with a single large pore structure. *Ceram Int* 49: 36446–36457. https://doi.org/10.1016/j.ceramint.2023.08.328
100. Xu ZH, Liao DJ, Jin SM, et al. (2025) Preparation of lightweight ceramsite from tungsten tailings: Performance regulation and formation mechanism. *Environ Prog Sustainable Energy* 2025: e70146. https://doi.org/10.1002/ep.70146
101. Wang CQ, Duan DY, Huang DM, et al. (2022) Lightweight ceramsite made of recycled waste coal gangue & municipal sludge: Particular heavy metals, physical performance and human health. *J Clean Prod* 376: 134309. https://doi.org/10.1016/j.jclepro.2022.134309
102. Li T, Fan J, Sun T (2021) Effective removal of methylene blue dye from water with nanocomposite ceramsites in a fixed-bed column. *Environ Technol* 42: 3807–3819. https://doi.org/10.1080/09593330.2020.1743368
103. Pei JN, Pan XL, Qi YF, et al. (2022) Preparation of ultra-lightweight ceramsite from red mud and immobilization of hazardous elements. *J Environ Chem Eng* 10: 108157. https://doi.org/10.1016/j.jece.2022.108157
104. Wang X, Liu L, Zhou H, et al. (2021) Improving the compressive performance of foam concrete with ceramsite: Experimental and meso-scale numerical investigation. *Mater Des* 208: 109938. https://doi.org/10.1016/j.matdes.2021.109938
105. Wang XA, Li WG, Huang YH, et al. (2023) Study on shape-stabilised paraffin-ceramsite composites with stable strength as phase change material (PCM) for energy storage. *Constr Build Mater* 388: 131678. https://doi.org/10.1016/j.conbuildmat.2023.131678
106. Li M, Zhou DY, Jiang YQ (2021) Preparation and thermal storage performance of phase change ceramsite sand and thermal storage light-weight concrete. *Renew Energy* 175: 143–152. https://doi.org/10.1016/j.renene.2021.05.034

107. Liu CY, Luan KY, Su J (2023) Study on post-fire resistance of ceramsite foamed concrete sandwich composite slabs. *Structures* 58: 105506. https://doi.org/10.1016/j.istruc.2023.105506
108. Wang HX, Zhu YP, Zhang SF (2017) Experimental study on thermal insulation performance of ceramsite concrete composite wallboard. *Jiangxi Build Mater* 2017: 4–5. https://doi.org/10.3969/j.issn.1006-2890.2017.14.003
109. Zeng L (2011) Thermal resistance test and thermal performance analysis of building walls with ceramsite concrete blocks. *J Hunan Univ Technol* 6: 61–65.
110. Li J, Gao GB (2021) Preparation and application of ceramsite concrete from papermaking sludge in lightweight self-insulating wall materials. *New Build Mater* 48: 154–157. https://doi.org/10.3969/j.issn.1001-702X.2021.02.035
111. Zhu HB, Fu ZH, Wang Y, et al. (2023) Study on splitting tensile strength of interface between the full lightweight ceramsite concrete and ordinary concrete. *Case Stud Constr Mater* 18: e01829. https://doi.org/10.1016/j.cscm.2023.e01829
112. Zhou HC, Yang ZF (2012) Design and application of structural lightweight aggregate concrete in Jinying Fortune Center Project. *Chongqing Archit* 11: 5–7. https://doi.org/10.3969/j.issn.1671-9107.2012.08.005
113. Sun JK, Li RYM, Jiao T, et al. (2023) Research on the development and joint improvement of ceramsite lightweight high-titanium heavy slag concrete precast composite slab. *Buildings* 13: 3. https://doi.org/10.3390/buildings13010003
114. Zhang SL, Yuan K, Zhang JM, et al. (2020) Experimental study on performance influencing factors and reasonable mixture ratio of desert sand ceramsite lightweight aggregate concrete. *Adv Civ Eng* 2020: 8613932. https://doi.org/10.1155/2020/8613932
115. Zhao JK, Yu KQ, Xue JX (2004) Fabrication of structural ceramsite concrete and its precast components. *Guangdong Build Mater* 58–59. https://doi.org/10.3969/j.issn.1009-4806.2004.07.028
116. Zheng WK, He DY, Li H, et al. (2020) The preparation and properties of a shell structure ceramsite. *Materials* 13: 1009. https://doi.org/10.3390/ma13041009
117. Bu CM, Yang HY, Liu L, et al. (2022) Quantification of ceramsite granules in lightweight concrete panels through an image analysis technique. *Materials* 15: 1063. https://doi.org/10.3390/ma15031063
118. Gao S, Huang KA, Chu WC, et al. (2023) Feasibility study of pervious concrete with ceramsite as aggregate considering mechanical properties, permeability, and durability. *Materials* 16: 5127. https://doi.org/10.3390/ma16145127
119. Li SJ, Cui HH, Wang HH, et al. (2023) Preparation and performance investigation of epoxy resin-based permeable concrete containing ceramsite. *Polymers* 15: 4704. https://doi.org/10.3390/polym15244704
120. He YJ, Li GF, Li HB, et al. (2018) Ceramsite containing iron oxide and its use as functional aggregate in microwave absorbing cement-based materials. *J Wuhan Univ Technol* 33: 133–138. https://doi.org/10.1007/s11595-018-1797-9
121. Song JP, Liu J, Jin X (2022) Experimental study on crack resistance and mechanical properties of ceramsite-rubber fiber shotcrete. *China Meas Test Technol* 48: 169–176
122. Chen Y, Hui QJ, Zhang HW, et al. (2020) Experiment and application of ceramsite concrete used to maintain roadway in coal mine. *Meas Control-UK* 53: 1832–1840. https://doi.org/10.1177/0020294020947134

123. Wang YR (2001) Experiment and application of haydite concrete in rock workings support. *Hydraul Coal Min Pipeline Transp* 3: 23–27. https://doi.org/10.14187/j.cnki.cn13-1185/tn.2001.03.008
124. Huang JK, Pang JY, Liu GC, et al. (2019) A new heat insulation shotcrete mixed with basalt and plant fibers. *Adv Civ Eng* 2019: 6376807. https://doi.org/10.1155/2019/6376807
125. Deng YS, Zheng YF, Zhang KQ, et al. (2023) New progress in R&D and application of lightweight and high-strength concrete. *J Lanzhou Jiaotong Univ* 42: 137–143. https://doi.org/10.3969/j.issn.1001-4373.2023.02.019
126. Li P, Li J, Fan L, et al. (2024) Experimental investigation into lightweight high strength concrete with shale and clay ceramsite for offshore structures. *Sustainability* 16: 1148. https://doi.org/10.3390/su16031148
127. Wang J, Feng P, Hao T, et al. (2017) Axial compressive behavior of seawater coral aggregate concrete-filled FRP tubes. *Constr Build Mater* 147: 272–285. https://doi.org/10.1016/j.conbuildmat.2017.04.169
128. Liu JM, Ju BY, Xie W, et al. (2021) Design and evaluation of an ultrahigh-strength coral aggregate concrete for maritime and reef engineering. *Materials* 14: 5871. https://doi.org/10.3390/ma14195871
129. Yuan J, He PD, Li HY, et al. (2022) Preparation and performance analysis of ceramsite asphalt mixture with phase-change material. *Materials* 15: 6021. https://doi.org/10.3390/ma15176021
130. Chen B (2017) Study on road performance of fly ash blended ceramsite concrete. Master theses, Chongqing Jiaotong University.
131. Han ZY (2018) Experimental study on road performance of fly ash blended ceramsite concrete under different mix ratios. *Fly Ash Compr Util* 3: 55–58.
132. Li YL, Xu MY, Li Q, et al. (2022) Study on the properties and heavy metal solidification characteristics of sintered ceramsites composed of magnesite tailings, sewage sludge, and coal gangue. *Int J Env Res Pub He* 19: 11128. https://doi.org/10.3390/ijerph191711128
133. Zheng XK, Zou MY, Zhang BW, et al. (2022) Remediation of Cd^{-}, Pb^{-}, Cu^{-}, and Zn^{-} contaminated soil using cow bone meal and oyster shell meal. *Ecotox Environ Safe* 229: 113073. https://doi.org/10.1016/j.ecoenv.2021.113073
134. Liu TW, Wang YM, Sun DS, et al. (2025) Research on the preparation and properties of ceramsite sand from desert sand synergistic multivariate industrial solid waste. *Constr Build Mater* 497: 143800. https://doi.org/10.1016/j.conbuildmat.2025.143800
135. Xu K, Zhan X, Wang Y, et al. (2025) All-solid-waste-based non-sintered ceramsite prepared from coal fly ash and dechlorinated municipal solid waste incineration fly ash: Performance and hydration mechanisms. *J Environ Manage* 395: 127906. https://doi.org/10.1016/j.jenvman.2025.127906
136. Li J, Yu G, Xie S, et al. (2018) Immobilization of heavy metals in ceramsite produced from sewage sludge biochar. *Sci Total Environ* 628–629: 131–140. https://doi.org/10.1016/j.scitotenv.2018.02.036
137. Tang KJ, An HN, Liu CB, et al. (2024) Safety and environmental protection application of high performance solid waste unburned ceramsite and its lightweight high strength concrete. *Sustain Chem Pharm* 40: 101611. https://doi.org/10.1016/j.scp.2024.101611

138. Hao XD, Chen Q, Li J, et al. (2019) No need to worry about tail gas pollutants from sludge incineration. *China Water Wastew* 35: 8–14. https://doi.org/10.19853/j.zgjsps.1000-4602.2019.10.002
139. Ling W, Xing Y, Zhao CW, et al. (2024) Research progress on exhaust gas emissions and control technology during sewage sludge thermal drying: A review. *Dry Technol* 42: 1–18. https://doi.org/10.1080/07373937.2023.2260895
140. Lin SD, Lu Y, Zheng L, et al. (2023) Immobilization potential of Cr through ultrasonic-assisted water washing in MSWI fly ash and evaluation of carbon capture and product reuse in its washing liquid. *Process Saf Environ* 174: 627–636. https://doi.org/10.1016/j.psep.2023.04.035
141. Qiu QL, Chen Q, Jiang XG, et al. (2019) Improving microwave-assisted hydrothermal degradation of PCDD/Fs in fly ash with added Na_2HPO_4 and water-washing pretreatment. *Chemosphere* 220: 1118–1125. https://doi.org/10.1016/j.chemosphere.2018.12.166
142. Yang JH, Dai GF, Peng C, et al. (2025) Preparation of lightweight and high-strength ceramsite by washed municipal solid waste incineration fly ash coupled with coal gangue: Phase transformation mechanism and pollution control. *J Environ Chem Eng* 13: 119294. https://doi.org/10.1016/j.jece.2025.119294
143. Zhang K, Liu SH, Zhang RX, et al. (2018) Research on preparation of non-sintered ceramsite from gasification cinder and its performance. *Coal Sci Technol* 10: 222–227. https://doi.org/10.13199/j.cnki.cst.2018.10.035

AIMS Press